

Empirical Tests of Pre–Main-Sequence Stellar Evolution Models with Eclipsing Binaries

Keivan G. Stassun^{a,b}, Gregory A. Feiden^c, Guillermo Torres^d

^a*Department of Physics & Astronomy, Vanderbilt University, 1807 Station B, Nashville, TN 37235, USA*

^b*Physics Department, Fisk University, 1000 17th Avenue North, Nashville, TN 37208, USA*

^c*Department of Physics & Astronomy, Uppsala University, Box 516, SE-751 20 Uppsala, Sweden*

^d*Harvard-Smithsonian Center for Astrophysics, 60 Garden Street, Cambridge, MA 02138, USA*

Abstract

We examine the performance of standard pre–main-sequence (PMS) stellar evolution models against the accurately measured properties of a benchmark sample of 26 PMS stars in 13 eclipsing binary (EB) systems having masses 0.04–4.0 M_{\odot} and nominal ages ≈ 1 –20 Myr. We provide a definitive compilation of all fundamental properties for the EBs, with a careful and consistent reassessment of observational uncertainties. We also provide a definitive compilation of the various PMS model sets, including physical ingredients and limits of applicability. No set of model isochrones is able to successfully reproduce all of the measured properties of all of the EBs. In the H-R diagram, the masses inferred for the individual stars by the models are accurate to better than 10% at $\gtrsim 1 M_{\odot}$, but below 1 M_{\odot} they are discrepant by 50–100%. Adjusting the observed radii and temperatures using empirical relations for the effects of magnetic activity helps to resolve the discrepancies in a few cases, but fails as a general solution. We find evidence that the failure of the models to match the data is linked to the triples in the EB sample; at least half of the EBs possess tertiary companions. Excluding the triples, the models reproduce the stellar masses to better than $\sim 10\%$ in the H-R diagram, down to 0.5 M_{\odot} , below which the current sample is fully contaminated by tertiaries. We consider several mechanisms by which a tertiary might cause changes in the EB properties and thus corrupt the agreement with stellar model predictions. We show that the energies of the tertiary orbits are comparable to that needed to potentially explain the scatter in the EB properties through injection of heat, perhaps involving tidal interaction. It seems from the evidence at hand that this mechanism, however it operates in detail, has more influence on the surface properties of the stars than on their internal structure, as the lithium abundances are broadly in good agreement with model predictions. The EBs that are members of young clusters appear individually coeval to within 20%, but collectively show an apparent age spread of $\sim 50\%$, suggesting true age spreads in young clusters. However, this apparent spread in the EB ages may also be the result of scatter in the EB properties induced by tertiaries.

Keywords: eclipsing binaries, stellar evolution, star formation

1. Introduction

1.1. Eclipsing binaries as tests of stellar models

Eclipsing binary (EB) stars have long served as fundamental benchmarks in stellar astrophysics. Through spectroscopic and photometric analysis of an EB, it is possible to empirically measure the fundamental physical properties of the component stars to a high degree of both precision and accuracy with almost no theoretical assumptions (e.g., Andersen, 1991). For example,

through radial velocities measured from a set of double-lined spectra, the component masses can be directly determined, with an accuracy of $\sim 1\%$ in the best cases (e.g., Morales et al., 2009). Indeed, the number of EBs with component masses and radii determined with an accuracy of better than 3% is now approximately 100 (Torres et al., 2010).

Such accurately determined stellar properties enable stringent tests of stellar models. For main-sequence EBs, these tests generally find that the models perform very well at masses $\gtrsim 1 M_{\odot}$, but at lower masses there are important discrepancies. For example, low-mass EBs exhibit systematically lower effective temperatures

Email addresses: keivan.stassun@vanderbilt.edu (Keivan G. Stassun), gregory.a.feiden@gmail.com (Gregory A. Feiden), gtorres@cfa.harvard.edu (Guillermo Torres)

(T_{eff}) and systematically larger radii (R) than predicted by standard stellar models (see, e.g., Torres & Ribas, 2002; Ribas, 2003; López-Morales & Ribas, 2005; Torres, 2013). This may be the result of the magnetic activity that is often observed among low-mass stars. While there is not yet a clear consensus in the literature as to the physical mechanism that drives the connection between activity, T_{eff} suppression, and R inflation, several studies have suggested that the effect can be empirically related to activity indicators such as $H\alpha$ and X-ray emission (e.g., López-Morales, 2007; Morales et al., 2008; Stassun et al., 2012). If correct, these relations might allow empirical corrections to be made to the inferred masses of active, low-mass stars, and they suggest that there are missing physical ingredients in standard models, most notably magnetic fields.

In the last 15 years, new generations of theoretical stellar evolution models including the effects of magnetic fields have been developed (D’Antona et al., 2000; Mullan & MacDonald, 2001; Feiden & Chaboyer, 2012b) that are better able to reconcile the observed T_{eff} and R of some observed low-mass EBs (MacDonald & Mullan, 2010, 2012; Feiden & Chaboyer, 2013). For instance, Feiden & Chaboyer (2012b) are able to successfully model the previously vexing EB EF Aqr by incorporating magnetic fields with strengths of 3–5 kG in their stellar models in a fully physically consistent fashion. Similarly, Feiden & Chaboyer (2013) find that YY Gem requires models with field strengths of several hundred Gauss driven by convective energy to reconcile the observed inflated R and suppressed T_{eff} .

At the same time, application of these new models questions the degree to which the observed properties for most EBs in fact systematically deviate from expectation. Potentially underestimated systematic errors in EB measurements and uncertainties in age and/or metallicity could be lurking in the data. Feiden & Chaboyer (2012a) find that more than 90% of the benchmark EBs they considered have properties fully consistent with the Dartmouth stellar models when the previously assumed EB ages and metallicities are carefully re-examined. For instance, the low-mass EB CU Cnc, considered a quintessential example of activity-inflated R , is found to in fact be well modeled by standard models if its age is several Gyr as opposed to the commonly assumed ~ 400 Myr; essentially, CU Cnc may not be a member of the Castor moving group as has been commonly assumed (Feiden & Chaboyer, 2013).

Thus, while the effects of magnetic activity appear to be important for some extremely active low-mass EBs (Stassun et al., 2012; Feiden & Chaboyer, 2012b,

2013), it is proving valuable to carefully reexamine the ability of standard stellar models to reproduce the majority of EBs when confronted with realistic observational uncertainties and more accurate priors on other relevant stellar properties, such as the stellar ages.

1.2. Pre-main-sequence eclipsing binaries

The complexity of the stellar physics intrinsic to low-mass stars is exacerbated for low-mass stars in the pre-main-sequence (PMS) phase of evolution. PMS stars are expected to be fully convective in the early stages of PMS evolution, making the difficult physics of convection central to the modeling problem. Very young stars are generally rapidly rotating, at least as compared to their main sequence counterparts which have begun to spin down, and thus almost always exhibit some indicator of strong magnetic activity (e.g., periodic variability attributed to spots, strong $H\alpha$ and X-ray emission, etc.; Stassun et al., 1999, 2004, 2006b), making any effects of strong surface magnetic fields ubiquitous. All PMS stars have presumably undergone a phase of vigorous accretion, if they are not still actively accreting, making any effects of previous accretion history salient (e.g., Baraffe et al., 2009; Simon & Obbie, 2009; Baraffe & Chabrier, 2010). Finally, PMS stars by definition have not yet established full main-sequence hydrostatic equilibrium and are still contracting. This contraction of PMS stars furthermore suggests that stars in close binary systems may have previously experienced strong(er) tidal interactions when the stars were even larger than observed at the present moment. Thus, from a modeling standpoint alone, PMS stars are complex, dynamic, and may be prone to effects from their recent evolutionary history (i.e., accretion, tides) that may or may not still be directly observable.

Observationally, PMS stars are challenging as well. During the first few Myr of evolution, many if not most PMS stars exhibit variability and complexities arising from active accretion (e.g., Herbst et al., 1994) that are difficult if not impossible to separate from magnetic activity. These stars are also frequently observed within larger star-forming regions that have strong nebular emission and that subject the individual stars to a highly dynamical environment including gravitational interactions with the other stars (e.g., Bate, 2009). Furthermore, the determination of basic stellar properties for PMS stars is often confounded by uncertain circumstellar and/or environmental extinction, uncertain distances, and even uncertainties in the T_{eff} scale and bolometric corrections. As a consequence, there remain ongoing debates in the literature as to the degree of coevality in young star-forming regions because of

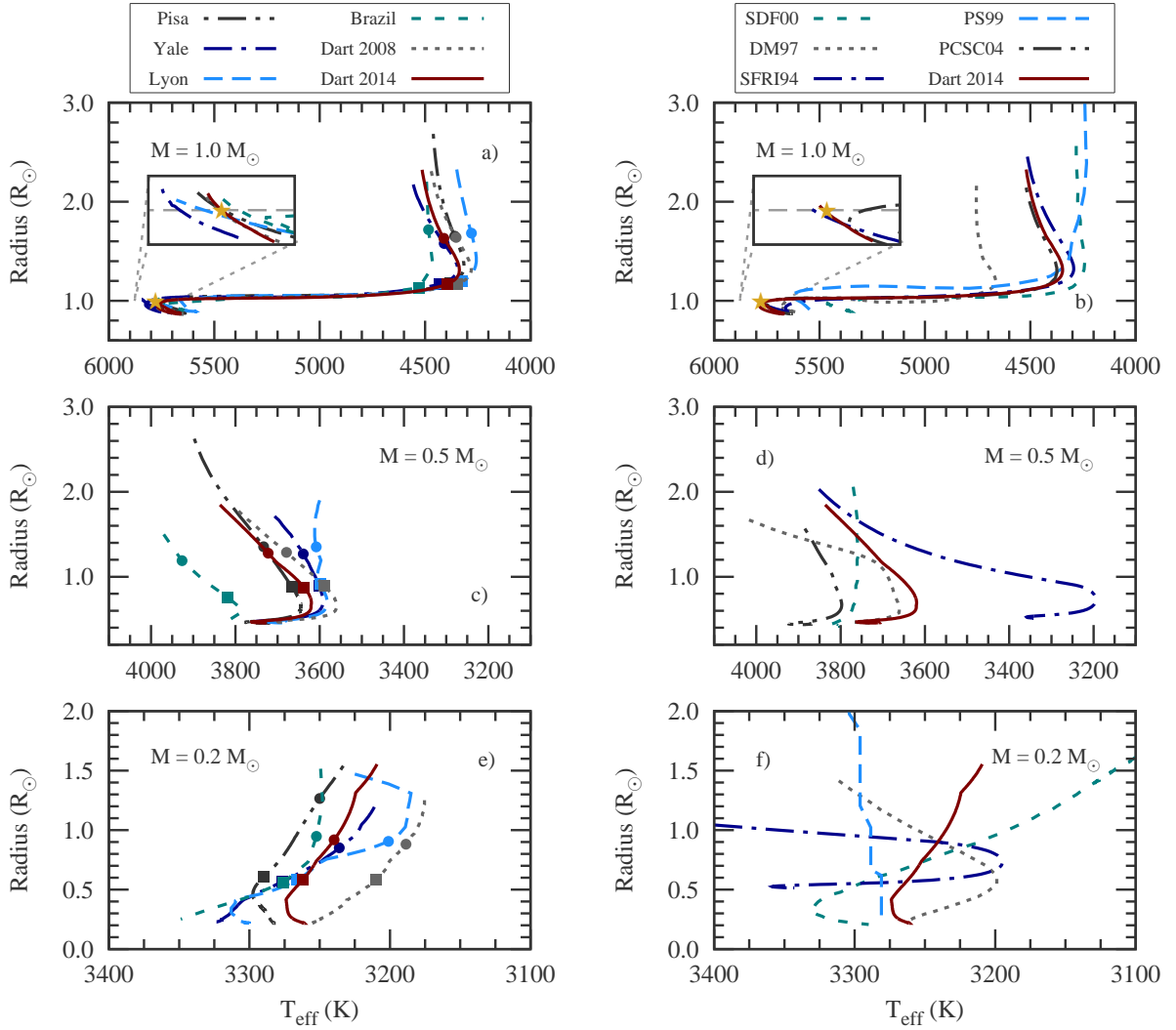


Figure 1: Model evolutionary tracks for stars of $1.0 M_{\odot}$ (a and b), $0.5 M_{\odot}$ (c and d) and $0.2 M_{\odot}$ (e and f). Left panels (a, c, e) display tracks for model sets adopted in the review, while right panels (b, d, f) show tracks from discarded model sets. The Dartmouth 2014 models are shown in both the left and right panels for reference. Each track begins at an age of 1 Myr and terminates on the main sequence. Yellow star symbols in the $1.0 M_{\odot}$ panels represent the Sun, and small insets highlight the quality of the solar calibration. Two ages, 3 Myr and 10 Myr, are marked along the adopted tracks with a solid circle and solid square, respectively.

large uncertainties in the observed stellar luminosities (e.g., Kraus & Hillenbrand, 2009; Da Rio et al., 2010; Jeffries et al., 2011).

Empirical testing and benchmarking of PMS stellar evolution models is important for multiple reasons. These models are the basis for the inferred masses and ages of the vast majority of young stars. Consequently, our understanding of basic stellar astrophysical ingredients, such as initial mass functions, depends on these models. Likewise, our understanding of the timescales for the dissipation of circumstellar disks and for the formation of planets around stars

relies entirely on the age scale implied by the models. But transforming the directly observed properties of young stars, such as temperatures and luminosities, into masses and ages using the current suite of theoretical PMS stellar models results in a factor of ~ 2 – 3 variation in mass and in age due to large differences in theoretical evolutionary PMS tracks (Figure 1, and see, e.g., Simon et al., 2000; Hillenbrand & White, 2004; Soderblom et al., 2013). For example, given a star with $R = 1.0 R_{\odot}$ and $T_{\text{eff}} = 3600$ K, PMS stellar evolution models listed in Tables B.6 and B.7 predict that star to have a mass of $0.33 M_{\odot}$ up to $0.60 M_{\odot}$ with an

age anywhere from 3 Myr to 10 Myr. Consequently, the predictions of PMS stellar models remain very much in need of benchmarking against accurate empirical measurements of PMS stellar properties.

Previous reviews of empirical constraints on PMS models include Young et al. (2001), Hillenbrand & White (2004), Mathieu et al. (2007), Tognelli et al. (2012), Gennaro et al. (2012), and Bell et al. (2012). Some of those reviews considered all PMS stars with dynamical mass determinations, including PMS EBs, PMS visual binaries with astrometric orbits, and single PMS stars with rotation curve measurements of their circumstellar disks. In this review, we focus exclusively on the sample of published, well characterized PMS EBs, as these provide direct measurements of both the stellar masses and the stellar radii, as well as additional empirical determinations of quantities such as mass ratios and temperature ratios that can be used as stringent constraints on stellar models.

Fortunately, the past decade has seen advances in the number of PMS EBs with which to perform such tests. Whereas the most recent review on PMS EBs (Mathieu et al., 2007) included only six PMS EB systems, as of this writing there are now 13 PMS EB systems published with suitably well determined properties (see Sect. 2). While only three of these (EK Cep, RS Cha, and V1174 Ori) have mass and radius measurements of such high accuracy as the ~ 100 main-sequence EBs included in the review by Torres et al. (2010), these systems collectively possess sufficiently well measured stellar properties to permit a quantitative assessment of the various PMS stellar model suites currently available. They also permit an assessment of the degree to which non-standard stellar physics may be required to improve the performance of the models. Moreover, EBs bring the added benefit of permitting one to test the stellar models in the context of coevality, or in turn to ascertain the degree to which non-coevality may exist in young binaries. Indeed, the sample of PMS EBs that we study includes members of at least two young clusters with very different ages (Orion Nebula Cluster at $\sim 1\text{--}2$ Myr, and h Persei at ~ 13 Myr) so that we may investigate the question of coevality also across multiple EBs within the same cluster.

Our aim in this paper is not principally to perform a comprehensive review of the literature on this subject (see previous reviews cited above). Rather, we aim to (a) objectively compile the fundamental properties of a benchmark sample of PMS EBs in one place as a resource to the community, (b) objectively compile the salient physical ingredients for the various PMS model

suites in one place so that the community may more easily compare and contrast them, (c) systematically compare the physical predictions of the models against the EB measurements, and (d) synthesize the results of these comparisons in an attempt to identify the most important physical effects that will be needed to make progress in understanding PMS stars and the efficacy of PMS stellar models.

The remainder of the paper is structured as follows: Sect. 2 presents the 13 PMS EBs that we use as our benchmark sample and describes the basis for their selection. Sect. 3 presents the various stellar model sets that we compare against the measurements, summarizes their physical ingredients and assumptions, compares them to one another, and describes the methods by which we compare them to the data. This section also includes our thoughts regarding which model sets should continue to be used and which should be retired. Sect. 4 presents the basic results of our attempts to fit the stellar models to the EB measurements, including an assessment of which model sets perform best in parameter spaces of particular interest to observers seeking to utilize the stellar models for determinations of basic properties for young stars, and includes an examination of activity effects and lithium abundances. Sect. 5 discusses these results and synthesizes them around a discussion of various observational issues that will need to be resolved as well as various astrophysical effects that future generations of stellar models may need to incorporate, including magnetic fields, tidal interaction, and accretion history. In Sect. 6 we end with a summary of our conclusions and recommendations, and briefly identify key directions and challenges for future progress.

2. Sample of PMS Eclipsing Binaries

In this paper, we will utilize a set of benchmark-grade EBs at PMS ages for comparison against various theoretical PMS stellar evolution models. We restrict our consideration to EBs that satisfy the following criteria:

1. At least one peer-reviewed paper has been published that includes at least a double-lined spectroscopic orbit solution providing the two EB component masses (M) and a light curve analysis providing the two EB component radii (R) and effective temperatures (T_{eff}).
2. The system includes at least one component whose properties place it definitively above the nominal zero-age main sequence (ZAMS), and where the discovery paper(s) identify the system as being likely PMS.

3. Component masses below $5 M_{\odot}$ with reported uncertainties less than 10%.

The EBs we selected from the literature satisfying the above criteria are summarized in Table 1 and shown in Figure 2. Since the sample is relatively small, we have allowed three exceptions to these criteria in cases of special interest. These are the systems V615 Per and V618 Per, which are essentially on the ZAMS but still young enough to provide useful tests, and MML 53, for which the individual radii have not been measured (although their sum has) but which has a determination of the Li abundance for both stars that constitutes a useful constraint on models.

We have carefully reviewed the primary references pertaining to each of the 13 EB systems in order to confirm that they are otherwise suitable as benchmark-grade comparisons to theoretical PMS evolution models, and notes pertaining to each one based on our review of the literature are provided in Appendix A. This final sample set for our analysis below comprises 26 individual components in 13 EB systems, with masses spanning the range $0.037\text{--}4.075 M_{\odot}$ and nominal ages of $\approx 1\text{--}20$ Myr.

Table 1 also includes the fundamental physical parameters of each EB, namely M , R , and T_{eff} , in order of primary star mass (M_A). We do not tabulate bolometric luminosity (L_{bol}) or surface gravity ($\log g$) as these can be calculated directly from M , R , and T_{eff} . We also provide the mass ratio ($q \equiv M_B/M_A$) and the difference in T_{eff} , as these quantities are usually directly determined from the EB radial velocity and light curve analysis. In particular, ΔT_{eff} is generally determined more precisely than the individual absolute temperatures. Finally, Table 1 also indicates whether the EBs possess known tertiary companions. The distance and nominal age for each system are collected in Table A.5 (Appendix A). These ages are assigned primarily based on cluster membership (for those EBs that are established kinematic members of young clusters or associations) or else are the nominal age provided in the original papers.

Note that two of the EBs (four stars) in our final sample set are members of the η Persei cluster with a nominal age of ≈ 13 Myr (e.g., Capilla & Fabregat, 2002), and three of the EBs (4 stars and 2 brown dwarfs) are members of the Orion Nebula Cluster (ONC) star-forming region with nominal age of $\approx 1\text{--}2$ Myr (e.g., Hillenbrand, 1997; Mayne & Naylor, 2008; Da Rio et al., 2010).

In Table A.5 we provide for each of these EBs some ancillary information that we will utilize in our analysis.

These data include $H\alpha$ equivalent widths (EWs) and luminosities ($L_{H\alpha}$), X-ray fluxes and luminosities (F_X and L_X), and the abundances of lithium, $\log N(\text{Li})$. $L_{H\alpha}$ and L_X can be used as tracers of chromospheric activity for assessing the impact of magnetic activity on the stellar properties, whereas Li can be used as an independent measure of the stellar age since Li is not yet fully depleted in most low-mass PMS stars.

3. Stellar Evolution Models Examined and Methods of Comparison to Measured Stellar Properties

In this section, we summarize the stellar evolution models against which we compare the sample of benchmark PMS EBs from Sect. 2. All of the published and publicly available model sets with specific applicability to PMS evolution for low-mass stars have been considered and are summarized in Tables B.6 and B.7. Each set of models includes a range of applicability and a set of physical ingredients and assumptions as summarized in Tables B.6 and B.7. For context, evolutionary tracks for $1 M_{\odot}$, $0.5 M_{\odot}$, and $0.2 M_{\odot}$ are illustrated in the $T_{\text{eff}}\text{--}R$ plane in Figure 1 and a representative set of isochrones are shown in Figure 2¹.

There exists a large number of stellar evolution codes, each typically designed to suit a particular application given that the physical conditions present inside stars vary over orders of magnitude in pressure and temperature. Additionally, physical inputs used in stellar evolution codes (e.g., equation of state, opacities, boundary conditions) are undergoing constant revision, and consequently so are the stellar evolution models. Our attempt at a near-comprehensive list of published stellar models with applicability to PMS evolution of low-mass stars is given in Tables B.6 and B.7.

We have endeavored to select a subset of the theoretical calculations that we believe are representative of what modelers might consider to be the current best effort at producing models with realistic physical inputs. We define the following set of criteria for the inclusion of a model set in our review:

1. Models are or will be publicly available.

¹The isochrones show an increase and then a decrease in radius as stars approach the ZAMS. The initial radius increase is a response of the stellar envelope to increased energy output from the $p\text{--}p$ chain and gravitational contraction of the core, producing greater ionization in the outer layers and thus reducing the size of the outer convection zone. Strong burning contributions from the CN cycle reverse the increasing radii by impeding core contraction and triggering formation of a convective core. Progress toward the ZAMS is temporarily halted as the CN cycle efficiency is reduced prior to ignition of nitrogen burning and equilibration of the complete CNO cycle.

Table 1: Fundamental properties of young EBs

Star	Per (d) V (mag)	Comp	Mass (M_{\odot})	Radius (R_{\odot})	T_{eff} (K)	$q \equiv M_B/M_A$ ΔT_{eff} (K)	Tertiary?
V615 Per	13.714	A	4.075 ± 0.055	2.29 ± 0.14	15000 ± 500	0.7801 ± 0.0098	N
	13.02	B	3.179 ± 0.051	1.903 ± 0.094	12700 ± 700	2300 ± 500	
TY CrA	2.889	A	3.16 ± 0.08	1.80 ± 0.10	12000 ± 500	0.5176 ± 0.0052	Y
	9.30	B	1.64 ± 0.04	2.08 ± 0.14	4900 ± 400	7100 ± 300	
V618 Per	6.367	A	2.332 ± 0.031	1.64 ± 0.10	11000 ± 1000	0.6682 ± 0.0087	N
	14.62	B	1.558 ± 0.025	1.32 ± 0.10	8100 ± 700	2900 ± 500	
EK Cep	4.428	A	2.025 ± 0.023	1.5800 ± 0.0065	9000 ± 200	0.5540 ± 0.0039	N
	7.85	B	1.122 ± 0.012	1.3153 ± 0.0057	5600 ± 200	3400 ± 150	
RS Cha	1.670	A	1.854 ± 0.016	2.138 ± 0.055	7640 ± 180	0.9798 ± 0.0056	Y?
	6.04	B	1.817 ± 0.018	2.339 ± 0.055	7240 ± 170	400 ± 30	
ASAS J052821+0338.5	3.873	A	1.375 ± 0.028	1.83 ± 0.07	5100 ± 100	0.9719 ± 0.0067	N
	11.71	B	1.329 ± 0.020	1.73 ± 0.07	4750 ± 180	350 ± 150	
RX J0529.4+0041	3.038	A	1.27 ± 0.01	1.44 ± 0.10	5200 ± 150	0.7305 ± 0.0025	Y
	12.35	B	0.93 ± 0.01	1.35 ± 0.10	4220 ± 150	980 ± 50	
V1174 Ori	2.635	A	1.006 ± 0.013	1.338 ± 0.011	4470 ± 120	0.7231 ± 0.0055	Y
	13.95	B	0.7271 ± 0.0096	1.063 ± 0.011	3615 ± 100	855 ± 50	
MML 53	2.098	A	0.994 ± 0.030	2.201 ± 0.071^a	4886 ± 100	0.863 ± 0.016	Y
	10.78	B	0.857 ± 0.026	...	4309 ± 100	...	
CoRoT 223992193	3.875	A	0.668 ± 0.012	1.295 ± 0.040	4000 ± 200	0.7417 ± 0.0074	N
	16.69	B	0.4953 ± 0.0073	1.107 ± 0.050	3750 ± 200	...	
Par 1802	4.674	A	0.391 ± 0.032	1.73 ± 0.015	3675 ± 150	0.985 ± 0.029	Y
	15.38	B	0.385 ± 0.032	1.62 ± 0.015	3365 ± 150	310 ± 40	
JW 380	5.299	A	0.262 ± 0.025	1.189 ± 0.175	3590 ± 150	0.577 ± 0.032	Y
	16.92	B	0.151 ± 0.013	0.897 ± 0.170	3120 ± 100	470 ± 70	
2MASS J05352184-0546085	9.780	A	0.0572 ± 0.0033	0.690 ± 0.011	2715 ± 200	0.639 ± 0.024	N
	13.47K	B	0.0366 ± 0.0022	0.540 ± 0.009	2850 ± 200	-135 ± 30	

^a Radius sum; the individual radii have not been determined for this system.

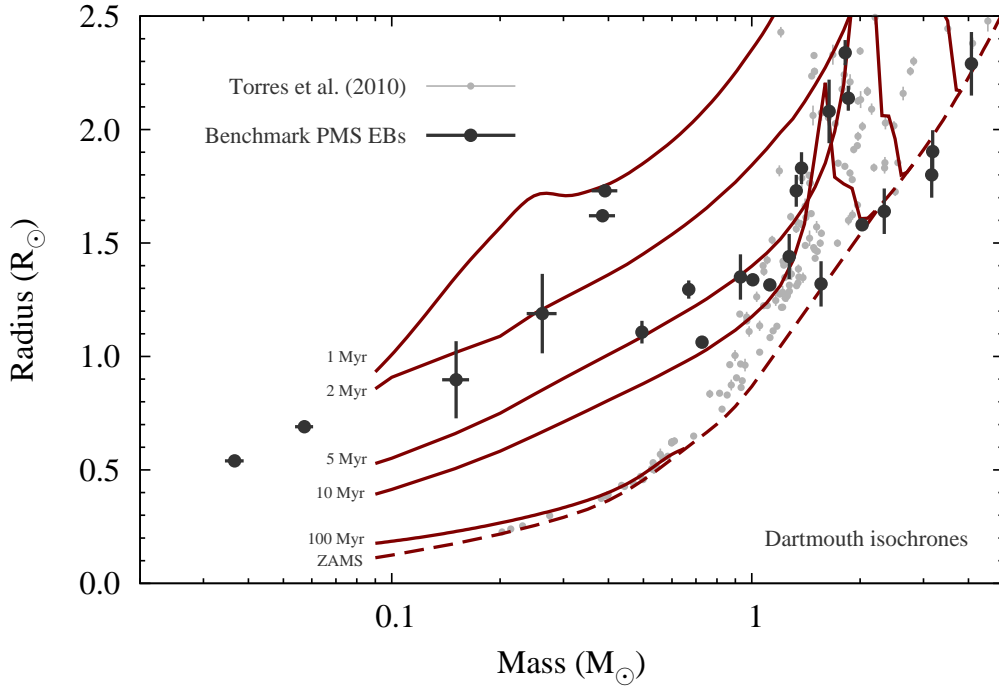


Figure 2: Overview of the benchmark EBs. Isochrones are from the Dartmouth 2014 series, black points are the benchmark EBs considered in this paper, and light grey points are the benchmark EBs from Torres et al. (2010). The zero-age-main-sequence (ZAMS) is shown as a dashed line. Noticeable features in the isochrones include the deuterium burning bump at low-masses around 1 Myr, and the rise and fall of stellar radii for stars with masses $\geq 1.2 M_{\odot}$ prior to the ZAMS (see Sec. 3).

2. Non-grey surface boundary conditions are used.
3. Models have been solar-calibrated (i.e., they reproduce the Sun’s properties at the solar age).

The series of models that meet these criteria are listed in Table B.6, while those that do not are listed in Table B.7. One may certainly debate these particular criteria as a global discriminant for adopting a given model set. For instance, it can be argued that there is no reason, *a priori*, to calibrate the convective mixing-length parameter to the Sun when the focus of the investigation is on cooler, PMS stars. Therefore our exclusion of certain model sets is not meant to suggest that these models are “wrong” or not suitable for use in certain contexts. Users of stellar models must carefully evaluate the applicability of any given model set to the problem at hand, based on the physical inputs and assumptions that went into the calculations. The information assembled in Tables B.6–B.7 is therefore intended as a guide to users who might otherwise have difficulty extracting this information readily from the original literature.

3.1. Physical Ingredients: Criteria

The characteristics of stellar evolution models listed above were selected as discriminants to optimize the va-

lidity of the adopted models across the mass regime spanned by our benchmark EBs. Surface boundary conditions defined by non-grey atmospheres are valid across the entire mass regime, from the sub-stellar regime up to the late-B-type stars. While grey atmosphere boundary conditions may be applied to higher mass stars ($> 0.9 M_{\odot}$) with relative accuracy, the same cannot be said of the lower mass population. Below roughly 5000 K it becomes increasingly important to adopt non-grey boundary conditions, as convection and radiation both play important roles in the transport of flux in the molecule-ridden cool star atmospheres. Therefore, while non-grey atmospheres would not be a limiting factor for the applicability of one model set against a given EB, a grey atmosphere would certainly provide a much less physically appropriate analysis against a low-mass star.

A similar argument can be made for the inclusion of modern opacity tables, although there has generally been widespread adoption of the latest opacity tables, so no model sets were excluded based on their adopted opacity data.

Solar calibration of stellar models is a continual source of debate. While few would argue against cal-

ibrating initial abundances of helium and heavy elements, the mixing length of convection is a highly contentious subject. For the purposes of this review, we sought to obtain a consistent sample of stellar models to permit a fair comparison based on minimal assumptions and as little tweaking of model parameters as possible. The simplest means of obtaining this sample is to adopt models that have been calibrated to the Sun.

This does raise a specific concern in the context of strong activity or magnetic field effects, which might cause departures from the solar convective calibration. For example, strong surface fields have been suggested to cause a reduction in surface convective efficiency (effectively, a reduction in the convective mixing-length parameter) for PMS stars. In our analysis, we first adopt the models with solar-calibrated convection, and then consider the possible effects of magnetic activity separately.

Lastly, it was required that models be publicly available. This criterion has nothing to do with the physical ingredients and is in no way indicative of the quality of a given model set. We enforced this criterion to make sure we were evaluating models that are more accessible to the wider community and therefore more likely to be adopted. Only in the case of the Montalbán et al. (2004) tracks did we find this to be a restriction. Most model sets having a large grid are publicly available.

3.1.1. Adopted Evolutionary Tracks

In Table B.6 we list the six model sets that satisfied our criteria above for inclusion: Baraffe et al. (1998, hereafter Lyon) models, Dotter et al. (2008, hereafter Dartmouth 2008) models, Landin et al. (2010, hereafter Brazil) models, Tognelli et al. (2011, hereafter Pisa) models, Spada et al. (2013, hereafter Yale) models, and Feiden et al. (in prep., hereafter Dartmouth 2014) models. These are also displayed in Fig. 1 (left panels). Note that the Dartmouth and Yale models are of the same lineage, both having developed from the Yale Rotating Evolution Code (Guenther et al., 1992). Despite their common lineage, the physics specific to low-mass stars developed independently, as evidenced in Table B.6. It is **also** important to note that while the Yale and Dartmouth 2008 models were not specifically designed for PMS studies, the physics included in the models are still valid in the PMS regime. Only at sufficiently young ages of around 1 Myr are there noticeable deficiencies in the adopted physics due to a lack of deuterium burning. The Brazil models are also available in a version that includes rotation (Landin et al., 2006, 2009), but we have adopted the non-rotating models for consistency with the other model sets.

3.1.2. Discarded Evolutionary Tracks

Stellar evolution model sets that did not satisfy the criteria for inclusion are listed in Table B.7 (and are also displayed in the right panels of Fig. 1). Some widely adopted stellar models are contained within this list, including the D’Antona & Mazzitelli (1997) and Siess et al. (2000) models. We recommend that use of these models should be approached with care. We briefly discuss why each of these model sets was excluded in Appendix B.

3.2. Inter-model Comparison

3.2.1. Mass Tracks

To illustrate how the various criteria affect the predictions of stellar models, we compare mass tracks and isochrones for all model sets in Figures 1 and 3. As shown in Figure 1(a, c, e), accepted mass tracks yield similar predictions at all masses. Noticeable differences for $1.0 M_{\odot}$ tracks occur at the youngest ages along the Hayashi track, typically before an age of 10 Myr, which is marked as solid square along each track. After 10 Myr, the model sets exhibit consistent properties on the nearly-horizontal Henyey track on the approach to the MS. A similar trend emerges at $0.5 M_{\odot}$, where the tracks produce nearly identical morphologies, but exhibit a spread in temperature of ± 50 K in T_{eff} along the Hayashi track near 3 Myr. This spread decreases to about ± 25 K after 10 Myr, just prior to the Henyey track. The mass track from the Brazil group is a noticeable exception, showing a systematically hotter temperature of about 175 K compared to the others.

At $0.2 M_{\odot}$, the spreads in T_{eff} are decreased to about ± 25 K along the mass tracks, with exception of the Lyon track at young ages near 3 Myr and the Dartmouth 2008 track, which is consistently 50 K cooler than the other tracks. We also see that the Dartmouth 2008, Yale, and Brazil tracks do not exhibit a hook toward a cooler T_{eff} shortly after 10 Myr as is characteristic of the other models. This can be understood, at least for the Dartmouth 2008 models, as a consequence of the fact that they attach the model atmosphere boundary conditions where $T = T_{\text{eff}}$. Though this has a minimal impact on the stellar radius predictions, T_{eff} values are typically cooler by 50 K compared to models that define the surface boundary conditions deeper within the star. Given this explanation, it is strange that the Brazil models do not exhibit this hook, as they report that boundary conditions are attached at an optical depth $\tau_{\text{fit}} = 10$. We are unable to confirm this for the Yale models, as they do not explicitly report the optical depth where boundary conditions are defined.

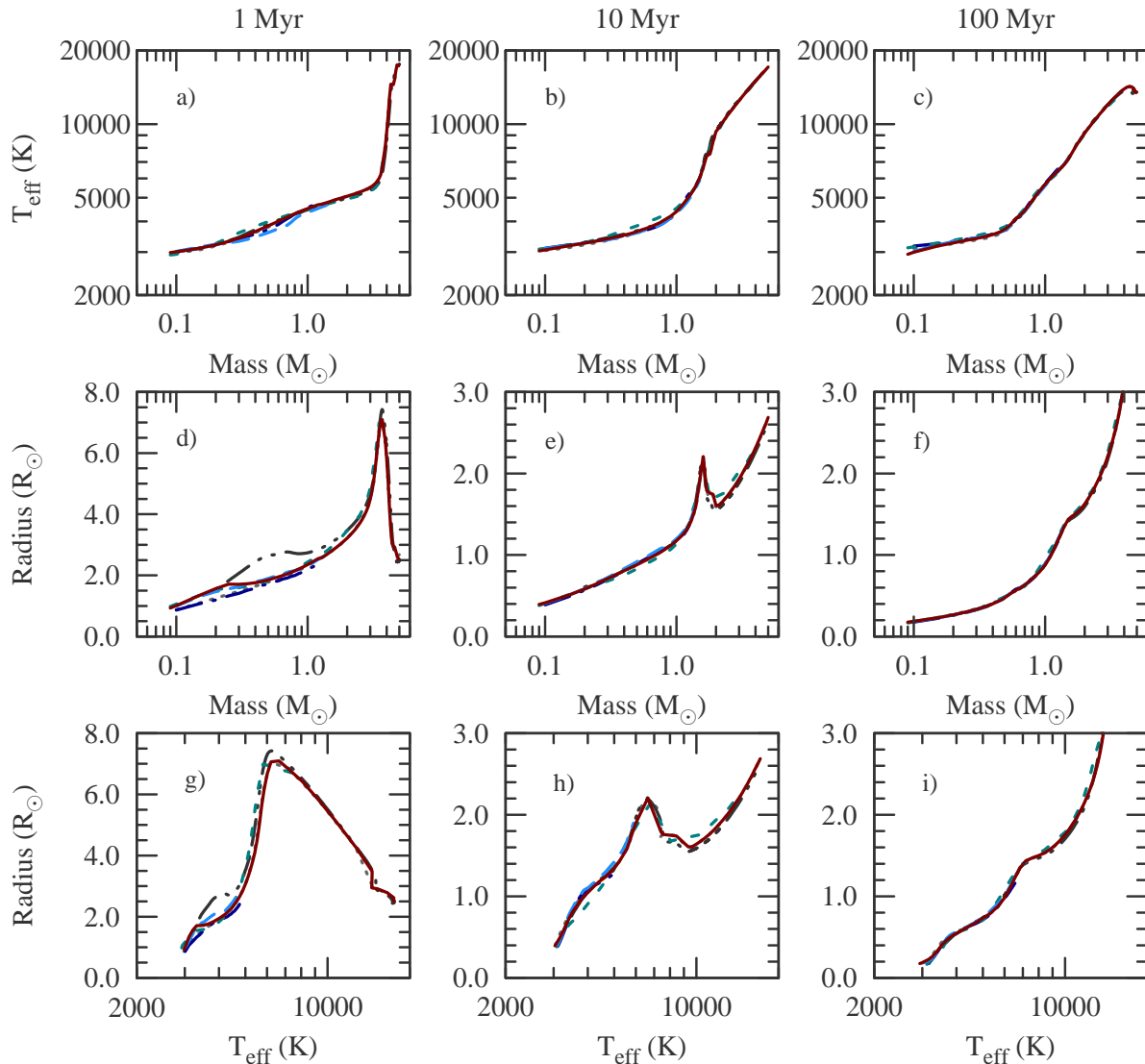


Figure 3: Comparison of accepted model isochrones at 1, 10, and 100 Myr in three different theoretical planes. Line styles represent the same stellar models as in Figure 1a): Brazil (green, short-dashed), Dartmouth (2014; maroon, solid), Dartmouth (2008; grey, dotted), Lyon (light-blue, long-dashed), Pisa (black, dash-double-dotted), Yale (dark-blue, dash-dotted). Panels a) – c) show the mass– T_{eff} plane, d) – e) show the mass–radius plane, and g) – i) show the T_{eff} –radius plane.

Among the discarded tracks, most of the $1.0 M_{\odot}$ tracks in Figure 1(b) exhibit similar behavior, as was the case for the included models. This is expected as boundary conditions play a less significant role at higher masses than they do for lower masses. One noticeable exception is the mass track from the D’Antona & Mazzitelli (1997) series, which is nearly 300 K hotter than the other models during contraction along the Hayashi track. Given the relative insensitivity of models to surface boundary conditions, this is a consequence of their non-local treatment of convection

with FST (Full Spectrum of Turbulence). Also of note in panel (b) is the lack of agreement with the Sun by the Siess et al. (2000) models. This is difficult to understand given that they did perform a solar calibration (Siess et al., 2000).

At lower masses, shown in Figures 1(d) and 1(f), the mass tracks begin to diverge significantly. Excluded models tend to have systematically hotter T_{eff} s at $0.5 M_{\odot}$, with the exception of the Swenson et al. (1994) track, which we do not attempt to explain. Hotter T_{eff} s are a consequence of adopting grey

boundary conditions, as has been discussed previously (Chabrier & Baraffe, 1997). At $0.2 M_{\odot}$ mass tracks again display a variety of morphologies. There are nearly as many different morphologies as there are mass tracks, a diversity caused largely by the different treatments of surface boundary conditions.

3.2.2. Isochrones

Figure 3 shows a comparison of solar composition isochrones at three ages for the adopted model sets. Isochrones from excluded models sets will not be discussed. In general there is good agreement between the different isochrone sets. This is not unexpected given the uniform selection criteria outlined in Sect. 3.1. At hotter T_{eff} s and higher masses, model sets predict very similar morphologies, although there are some noticeable offsets between 6300 K and 8000 K in the R - T_{eff} plane that correspond to the ignition of the CN cycle at lower temperatures and the nitrogen-burning bump at higher temperatures. The latter signals the CNO cycle coming into equilibrium with the ignition of nitrogen burning. These offsets appears to stem most from radius differences exhibited in panels (d) – (e). Significant variations between the model sets applicable in this temperature regime disappear by the age of 100 Myr as all of the higher mass stars have fully reached the main-sequence.

There is near unanimous agreement between the various model sets in the solar mass regime ($T_{\text{eff}} \sim 4300$ K at 1 and 10 Myr and $T_{\text{eff}} \sim 5500$ K at 100 Myr). The Pisa models show systematically larger radii at 1 Myr, but this difference vanishes by 10 Myr and suggests initial conditions are still important to consider at this age. Around 10 Myr, the Lyon models have simultaneously larger radii and cooler T_{eff} s by about 2% each, in the vicinity of $1.0 M_{\odot}$. Though small, the differences are at odds with the other model sets, which agree to within 0.5%. By 100 Myr, all model sets agree to within 0.3%. We have no precise explanation for the larger radii and cooler T_{eff} s of the Lyon models at early times, but it may be related to a combination of the depth at which the surface boundary conditions are fit and the adopted heavy element composition (for a thorough discussion see Tognelli et al., 2011). The Lyon models adopt the Grevesse & Noels (1993) heavy element composition and fit their surface boundary conditions at an optical depth $\tau_{\text{fit}} = 100$. In contrast, the other model sets adopt an overall lower heavy element abundance, at least for the interior composition (Grevesse & Sauval, 1998; Asplund et al., 2005), and fit the surface boundary conditions at lower optical depths (see Table B.6 for details).

Differences at low masses are more difficult to discern from the panels in Figure 3 as large relative variations in the predicted fundamental properties translate to small absolute variations. However, we observe several differences among the different groups. First, the Pisa models show a large radius offset (up to 35%) at 1 Myr. This feature seems to be a consequence of the model initial conditions, which set the age when deuterium burning occurs; at 1 Myr, deuterium burning appears to extend to higher masses in the Pisa models than in the others. It is difficult to assess which, if any, of the models in this regime are correct based on purely theoretical arguments. However, it is important to be cautious of models at this age, as they do not “forget” their initial conditions until sometime between 1 and 10 Myr (Baraffe et al., 2002). In the same manner, the Lyon isochrone at 1 Myr appears cooler than the others at a given mass. By 10 Myr the temperature difference disappears, but a slight radius offset is still present before the tracks come into agreement with the other sets around 100 Myr. One also notices in panel (d) that the Yale and Dartmouth 2008 isochrones are cooler than the others. This is a consequence of the absence of deuterium burning in these model sets.

Also difficult to discern from the isochrones are deviations of the Brazil, Yale, and Dartmouth 2008 models at the lowest masses at 100 Myr. These isochrones exhibit a different concavity between 0.1 and $0.2 M_{\odot}$, or $T_{\text{eff}} \approx 3500$ K. In addition, the models show a milder slope in panel (c), corresponding to a steeper slope in panel (i) below 3200 K. These features are very likely the result of surface boundary conditions being attached in regions of the star where convection is sufficiently non-adiabatic that detailed radiative transfer from non-grey models are required.

3.3. Methods of Fitting and Comparison against EB Data

Previous comparisons of stellar models to observed stellar properties have often been performed in the H-R diagram plane, i.e., fitting model isochrones to the observed T_{eff} and L . Here, the benchmark PMS EBs were fit to stellar evolution isochrones using six of the most accurately directly measured stellar properties: the primary mass, the mass ratio of the secondary to the primary, the primary and secondary radii, the primary T_{eff} , and the T_{eff} difference between the two components. Throughout this review we refer to the “primary” as the star with the larger measured mass, and we consider only models with solar composition. We sought the best isochrone within a given model set that simultaneously fit the two stars in a given EB; thus this test

implicitly assumes coequality for the two stars in the system. Isochrones provided by the various groups were used without any additional modifications, when possible. However, some models (i.e., Dartmouth 2008, Yale, and Brazil) do not include a sufficiently young or a sufficiently well-spaced set of isochrones in the target age range (1–100 Myr). We therefore computed isochrones from their evolutionary tracks with an age resolution of 0.2 Myr from 1 to 20 Myr, and 5 Myr from 20 to 100 Myr. While the isochrones are not specifically provided at these ages by the model grids, interpolation is a standard procedure when applying the model grids to observed properties of young stars.²

Each EB was fit to a given isochrone grid using the following procedure. First, the mass spacing along each isochrone was standardized to a resolution of $0.001 M_{\odot}$ to provide adequate sampling within one standard deviation of the quoted EB masses. Linear interpolation was sufficient as the original mass resolution was around $0.05 M_{\odot}$ for most model sets. Next, for a given isochrone, the two stars of the EB were compared to each mass point along the isochrone, with residuals in the mass, radius, and T_{eff} being calculated. To gauge the quality of fit, a goodness of fit statistic for each star was computed, as well as a global fit statistic for every combination of primary and secondary mass. We chose to use a χ^2 statistic,

$$\chi^2 = \sum_{i=1}^N \left(\frac{\delta X_i}{\sigma_{X,i}} \right)^2. \quad (1)$$

where $X_i \in \{M_A, q = M_B/M_A, R_A, R_B, T_{\text{eff},A}, \Delta T_{\text{eff}} = T_{\text{eff},A} - T_{\text{eff},B}\}$ is one of the defined properties used in the fit, δX_i is the difference between the observed and model isochrone value, $\sigma_{X,i}$ is that property’s associated observational uncertainty, and N is the total number of parameters being fit. The χ^2 statistic has the advantage of being an uncertainty weighted measure of the goodness of fit, thus forcing the isochrones to fit quantities that are the most precise.

A best fit pair of points along the isochrone, representing the primary and secondary star of the EB, was determined by locating the global χ^2 minimum among all of the possible combinations. This procedure was repeated for each isochrone of a given model set, yielding a list of the best fit primary and secondary masses at a given age. To find the overall best fit isochrone for a given EB, the global χ^2 minimum among this data set

²We chose not to request more extensive grids from authors of the models so as to preserve the principle of using only publicly available models.

was determined. We enforced strict coequality; the goodness of fit was determined by a single isochrone at a time for both stars simultaneously. Possible age spreads are considered in Sect. 4.5. The procedure was performed for each EB component using a restricted mass range along an isochrone between 5σ below and 5σ above the observed mass. We chose 5σ as a cut-off to allow the models sufficient flexibility in finding a best fit, while minimizing computational time spent performing comparisons between mass points that would be guaranteed to have a $\chi^2 > 150$, and thus not likely to be the location of a global χ^2 minimum in our fitting routine. We tested that this restriction did not introduce any biases in our results by comparing results of runs with and without the mass clipping for the Dartmouth models. No differences in the global minima occurred.

4. Results: Comparison of Models versus PMS EB Measurements

4.1. Recovery of stellar masses in the H-R diagram

Following previous reviews on the subject, we begin by considering the question: how reliably may one expect to determine the mass of a PMS star using the available stellar models? We perform this assessment from the “observer’s perspective,” that is, by considering what stellar masses one would infer for each EB star if it were “observed” in the H-R diagram and then compared to various stellar isochrones (Figure 4).

To perform this test, we searched for the best fit T_{eff} and L combination by minimizing the total χ^2 . Isochrones were searched within 1σ of the quoted T_{eff} . This is similar to the approach in Hillenbrand & White (2004) and Mathieu et al. (2007), but here explicitly accounting for the observational uncertainties in T_{eff} and L . Best fit χ^2 values were in all cases ≈ 0.0 as expected for a fit of two free parameters (mass, age) to two constraints. We then selected the mass at which the minimum χ^2 was found and compared it to the dynamically measured mass. Each star was treated individually; we did not enforce coequality. This in essence treats each individual star as though it were observed on its own.

The results are shown in Figure 5, in which we compare, for each of the models, the dynamically measured stellar masses to the masses inferred by the model isochrones from the observed T_{eff} and L in the H-R diagram. We show the primary stars and secondary stars separately. There is an apparent trend in most of the model sets in the sense that the models over-predict the masses, and this tendency increases toward the lowest masses. Interestingly, the tendency to over-predict

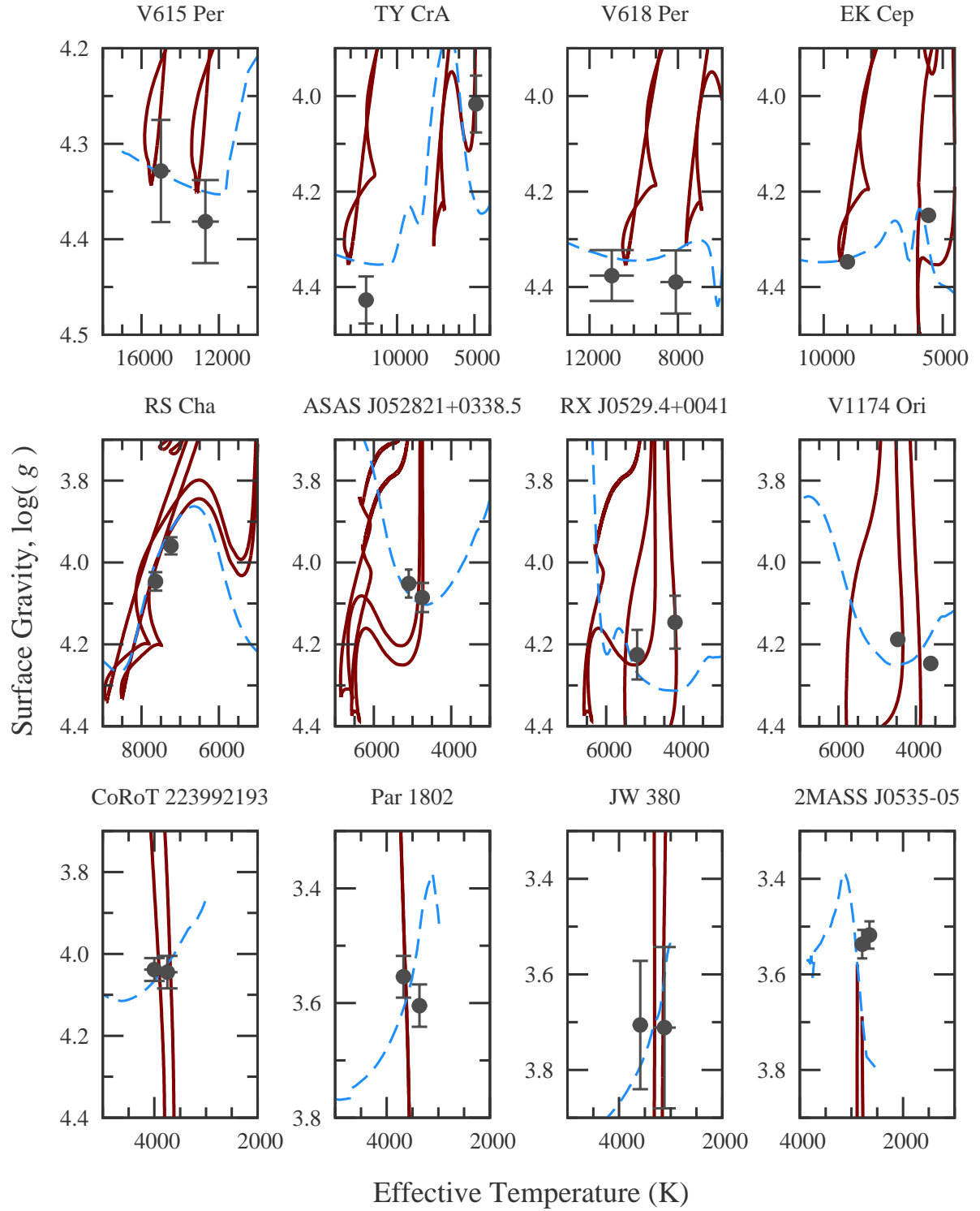


Figure 4: Fitting results for each of the benchmark EBs in a $T_{\text{eff}}-\log g$ HRD against Dartmouth 2014 mass tracks (maroon, solid lines) and isochrones (light-blue, dashed lines). Mass tracks were computed at the observed masses listed in Table 1 while isochrones are shown at the best fit age determined in Section 4.2.

the masses is most prominent among the primary stars; the secondaries appear fairly well distributed around the zero-point. However, the secondaries do in all of the models exhibit a larger dispersion.

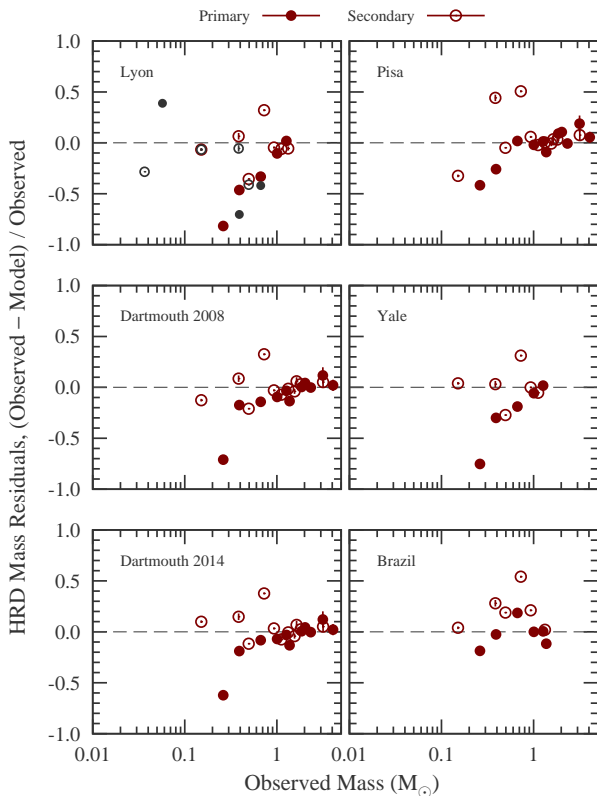


Figure 5: Mass residuals found from fitting observed PMS EB systems to models in the H-R diagram. Each panel shows the fit results for a different model suite, with primary and secondary stars shown with different symbols as labeled. For the Lyon model comparison (upper left), dark symbols represent the models with non-solar $\alpha_{\text{MLT}} = 1.0$, which are the only models that extend below $0.1 M_{\odot}$ to fit the brown-dwarf EB, 2M 0535–05.

The mean of the residuals and the r.m.s. deviations of the primaries and secondaries (taken together) for each of the model sets are summarized in Table 2. We divide each of the comparisons at $1 M_{\odot}$ to convey the degree to which the lower mass stars are more poorly reproduced. The Dartmouth models appear to exhibit the lowest overall scatter. The Pisa models show a slightly larger dispersion than the Dartmouth models at low masses, but have a comparable dispersion above $1 M_{\odot}$. The Brazil models do not show the trend mentioned above of increasingly over-predicted masses toward lower masses, but they do show a larger dispersion than the Pisa and Dartmouth models.

To be clear, this comparison is not quite fair to the stellar models, because it conflates any observational

biases with true astrophysical effects, as we discuss below. However, to the extent that the problem of inferring stellar masses from direct observables such as T_{eff} and L may be similarly affected by both observational and astrophysical effects not represented in the stellar models, this comparison provides a fair basis for quantifying the total errors that one may reasonably expect in such mass estimations.

In summary (see Table 2 and Figure 5), the accuracy with which one may expect to infer the true stellar mass above $1 M_{\odot}$ is for most of the model sets quite good, typically 1–10% in the mean, <10% scatter, and without obvious systematics (though the sign of the mean offsets does tend to indicate slightly over-estimated masses by the models). Below $1 M_{\odot}$, the situation is markedly worse, with offsets and scatters of $\sim 40\%$, and with a strong systematic tendency by most of the models toward over-estimated masses, the over-estimation approaching $\sim 100\%$ at $0.1 M_{\odot}$ (Figure 5). One exception to this trend is the Brazil model set, which yields no large mean offset (an absolute mean deviation of 15%) and a modest scatter of 22%. In any event it is clear that in general the H-R diagram inferred masses with all of the model sets are highly reliable above $1 M_{\odot}$ but moderately to highly unreliable below $1 M_{\odot}$.

We note that these findings differ qualitatively from those of Hillenbrand & White (2004) and Mathieu et al. (2007), who similarly found generally good agreement above $1 M_{\odot}$, but below $1 M_{\odot}$ found a tendency for the models to *under*-predict masses. Note however that these previous studies used mainly non-EB PMS stars with masses determined via astrometric orbits or circumstellar disk rotation curves. Only three of the EBs in our sample are in common across these studies, and for these three EBs we find very similar results as did those studies. In addition, the previous studies considered mainly previous generation PMS models—the Pisa, Brazil, and Dartmouth models were not yet available—and in this study we have excluded most of the model sets used in the previous studies for their use of grey atmospheres and/or their lack of solar calibration. As a result, only the Lyon models are in common to this study and the Hillenbrand & White (2004) and Mathieu et al. (2007) reviews. Therefore, with a largely different set of benchmark EBs and a largely different set of models considered, it may not be surprising that we find qualitatively different results in the ability of the models to recover the stellar masses in the H-R diagram.

However, as discussed below, this is not the last word, as there are important physical effects to consider that substantially alter the assessment of model performance in the H-R diagram, a question to which we return in

Table 2: Statistics of HRD fit for high- and low-mass populations.

Model set	Low-Mass Stars ($M < 1.0 M_{\odot}$)			High-Mass Stars ($M \geq 1.0 M_{\odot}$)		
	Mean	Abs. Mean	σ	Mean	Abs. Mean	σ
Brazil	0.154	0.207	0.218	-0.023	0.035	0.063
Dartmouth 2008	-0.123	0.225	0.295	-0.004	0.051	0.067
Dartmouth 2014	-0.044	0.209	0.293	-0.002	0.050	0.065
Lyon, $\alpha_{\text{MLT}} = 1.0$	-0.342	0.439	0.471
Lyon, $\alpha_{\text{MLT}} = 1.9$	-0.212	0.308	0.353	-0.050	0.060	0.051
Pisa	-0.003	0.259	0.339	0.033	0.053	0.069
Yale	-0.141	0.237	0.317	-0.031	0.043	0.042

Note: For the statistics compiled in the table, “Mean” refers to the direct mean fractional mass error, “Abs. Mean” is the mean absolute fractional error, and σ is the standard deviation about the mean computed using $N - 1$ in the denominator to compensate for the small sample size.

Sect. 5.5.

4.2. Detailed fitting of individual systems

As a more stringent and accurate test of the stellar models, we have gone beyond the H-R diagram plane and have fit each of the model isochrones to six of the directly measured properties for each EB, as described in Section 3.3.

An illustration of the quality of the fit of stellar evolution models to the observations for each of the 13 EBs may be seen in Figure 6, in which we show the residuals (observed minus predicted) for each of the fitted quantities normalized to their corresponding observational errors. The vertical dashed lines represent $\pm 3\sigma$ limits. In each case we have compared the six observables against all models from Table B.6 that allow the comparison (e.g., that have a suitable mass range), and we have represented each model with a different symbol. For MML 53 the individual component radii have not been measured, nor is an accurate temperature difference available. Consequently the constraint on models is considerably weaker than for other systems, which results in an artificially good match to predictions with a low χ^2 value. We therefore do not consider this system in the discussion below.

The two incarnations of the Dartmouth models yield very similar residuals in most cases, which is not surprising given that the physical ingredients are largely the same. In general the normalized residuals from all other models are also quite comparable, though there are exceptions such as the case of EK Cep, in which the Pisa and Brazil calculations deviate in opposite directions

compared to those from Dartmouth. Somewhat more than half of the systems may be considered to be reasonably well fit by the models, with all normalized residuals under 3σ . V615 Per, V618 Per, and CoRoT 223992193 are particularly well matched. On the other hand, all models have great difficulty fitting V1174 Ori, as well as Par 1802 to a lesser degree, though they all fail in similar ways hinting at either a common shortcoming in the physics of the models or perhaps unrecognized systematic errors in one or more of the measured quantities for those EBs. These two systems, along with EK Cep, happen to be the ones with the smallest formal relative errors in the individual radii, all at or under 1%. If those errors have been underestimated, they could explain the larger residuals from the fit in these cases.

The overall results of these fits are visually summarized in Figure 7, in which we plot the total system mass as a function of the χ^2 of the best fit isochrones. There is a hint of a tendency for the highest-mass EBs to be relatively well fit and for the lowest-mass EBs to be more poorly fit, although a larger sample is highly desirable to confirm this. Certainly there are some relatively high-mass systems that are as poorly fit as the lowest-mass systems. Thus, while the source of the system-to-system discrepancies with the model predictions may be mildly dependent on system mass, evidently the discrepancies are caused principally by other effects that we have not yet considered.

In Table 3 we list the best-fit ages we obtain for each EB and each set of models. In general the scatter among the different models for any given EB is typical of what is seen in the literature, and the mean ages are also con-

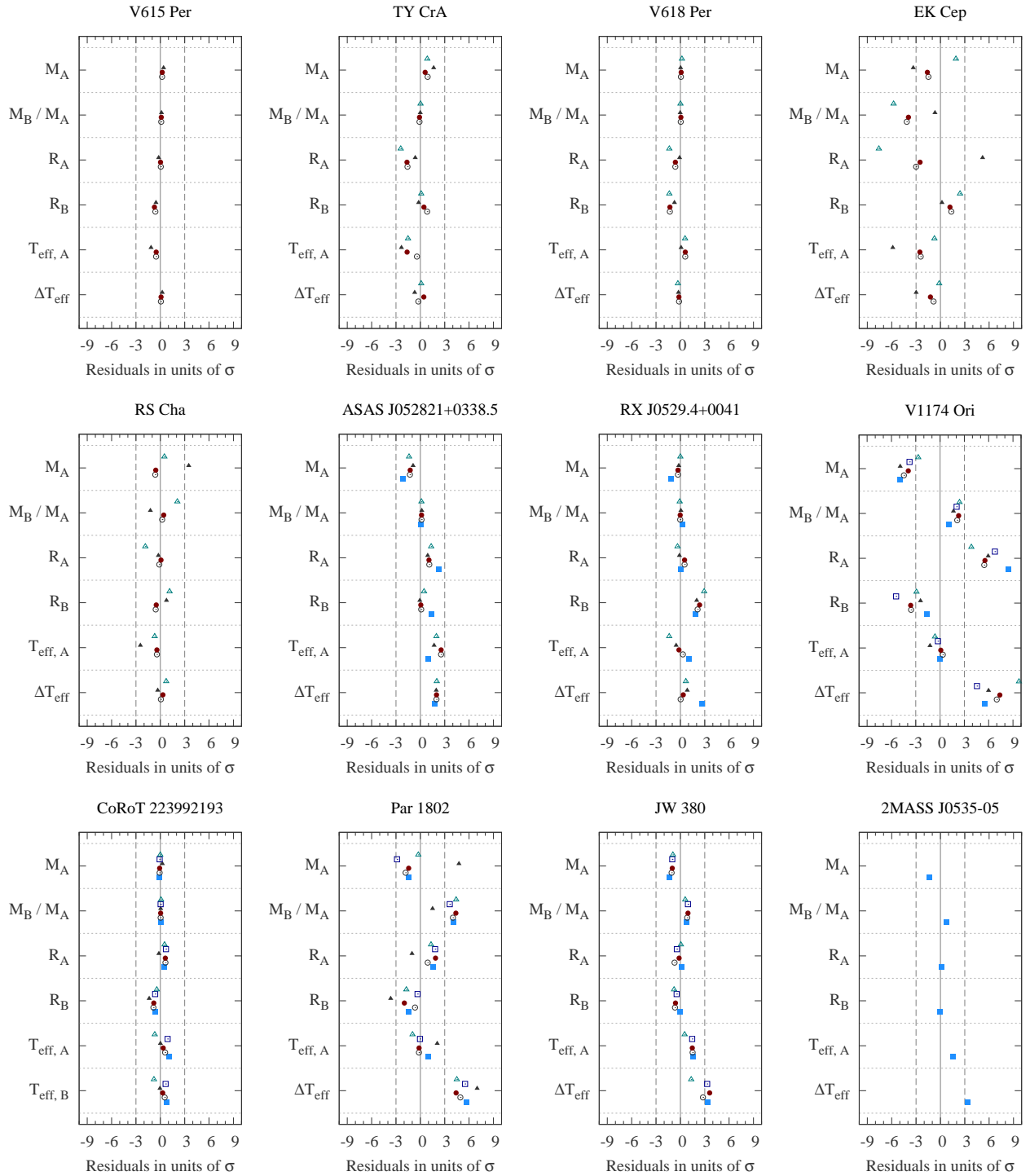


Figure 6: Fitting results for each of the benchmark EBs. Each model isochrone set (represented by different symbols) was fit to the six measured EB properties shown along the vertical axis. Note that for CoRoT 223992193 we used $T_{\text{eff},B}$ instead of ΔT_{eff} as the temperature difference has not been reported. The horizontal axis shows the residuals of the best-fit isochrone in the sense of (data – model), in units of the observational uncertainty, σ . Symbols are as shown in the legend of Figure 7. Note that for the brown-dwarf EB, 2M0535–05, only one set of models was applicable: the Lyon $\alpha_{\text{MLT}} = 1.0$ models.

Table 3: Best fit ages (Myr)

EB	Lyon	Dart 2008	Dart 2014	Pisa	Yale	Brazil	Gennaro [†]
V615 Per	...	4.7	4.9	15.0
TY CrA	...	3.6	7.7	7.0	...	7.6	3.75
V618 Per	...	25.0	25.0	30.0	...	19.8	...
EK Cep	...	20.0	19.4	19.0	...	18.8	18.95
RS Cha	...	7.7	7.7	7.0	...	7.8	8.00
ASAS J052821+0338.5	6.3	4.1	4.0	4.0	...	4.6	3.45
RX J0529.4+0041	10.0	10.4	10.8	9.0	...	11.8	6.90
V1174 Ori	10.0	8.2	7.8	8.0	7.8	7.0	7.40
MML 53	20.0	17.4	16.3	13.0	15.2	13.6	...
CoRoT 223992193	5.0	4.3	4.2	4.0	4.4	3.8	...
Par 1802	1.3	1.0	1.1	1.0	1.0	1.0	...
JW 380	2.5	1.4	2.1	...	1.4	2.0	...
2MASS J05352184-0546085	1.0

[†] Quoted ages are from Gennaro et al. (2012), who used Bayesian statistics to derive a best fit age for each system. Uncertainties are not listed here. Ages were computed assuming Gaussian mass priors.

sistent with previous estimates. In particular, the three EBs in the ONC display ages of 1–2 Myr (their canonical values). V615 Per and V618 Per, on the other hand, are not as consistent with their nominal age of ~ 13 Myr. The first system seems considerably younger according to the Dartmouth models, but not according to the Pisa models. All model sets give ages for V618 Per significantly older than 13 Myr. The reasons for these discrepancies are not obvious, although we note that Southworth et al. (2004) found these two EBs to be better fit with a lower metallicity than solar. Finally, we list the ages determined by Gennaro et al. (2012) for six of the EBs using a Bayesian analysis, finding that in general these Bayesian determined ages are consistent with the ages determined from our χ^2 minimization.

4.3. Fitting including empirical corrections for activity

Being young, many of the stars in our PMS EB sample exhibit clear signs of magnetic activity in the form of strong $H\alpha$ and X-ray emission (Table A.5). PMS stars may also exhibit strong $H\alpha$ emission if they are actively accreting. However, each of the EBs in our sample appears to be devoid of circumstellar material (with the exception of CoRoT 223992193), probably because in order to be observed as an EB at all the system cannot have a massive disk which would be viewed edge-on and consequently obscure the central EB.

To examine the degree to which chromospheric activity effects might be responsible for the poor agreement between the observed stellar properties and the theoretical stellar models for some of the systems, we have attempted to correct the directly observed T_{eff} and R values to what they would be if the stars were totally inactive. We converted the observed $H\alpha$ equivalent widths and X-ray fluxes F_X to luminosities ($L_{H\alpha}$ and L_X) using the distances in Table A.5, and in turn converted these into corrections to the stellar radii (δR) and temperatures (δT_{eff}) using the empirical relationships proposed by Stassun et al. (2012). Note that the Stassun et al. (2012) empirical relations are based on active main-sequence field dwarfs and active main-sequence EBs, and have not been broadly tested in the context of PMS stars (see also Sec. 5.1).

To convert $H\alpha$ equivalent widths to $L_{H\alpha}$ we used standard NextGen stellar atmospheres (Hauschildt et al., 1999a) to compute the surface continuum fluxes near $H\alpha$ and multiplied these by the stellar surface areas (using the measured R) and by the observed $H\alpha$ equivalent width. In cases where only a single, combined $H\alpha$ equivalent width was reported for an EB, we assumed that each component has the same intrinsic EW (equivalent to scaling the observed EW by each star’s L_{bol} and then correcting each star’s equivalent width for the continuum dilution by the other star). To convert F_X

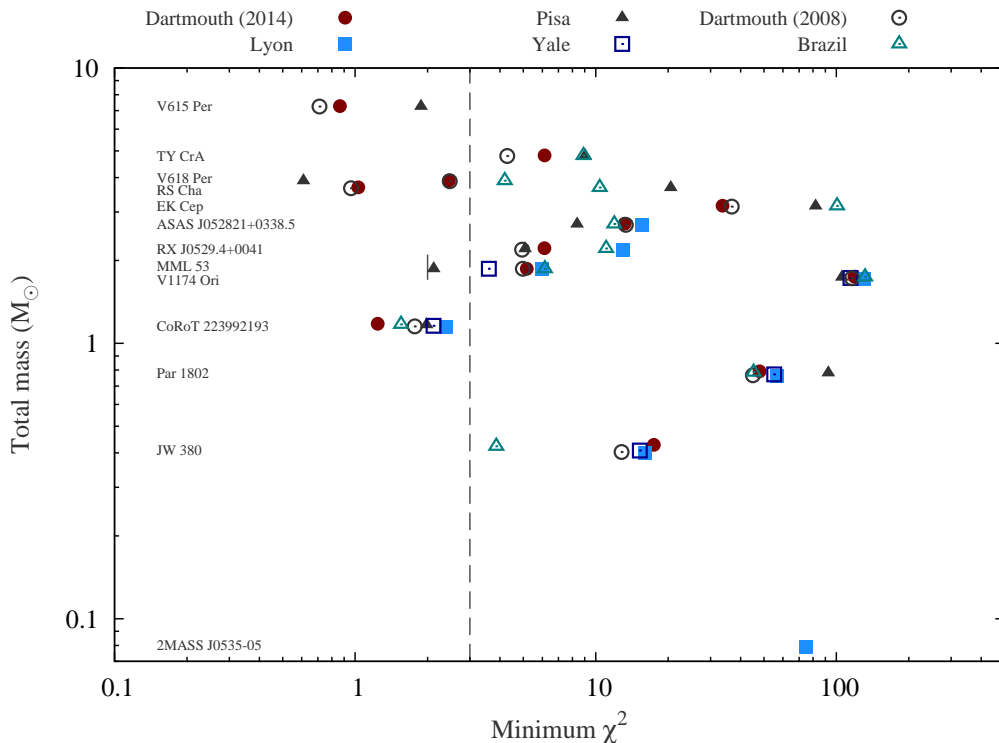


Figure 7: Total χ^2 of model isochrone fits (from Figure 6) versus total EB system mass. The vertical line at $\chi^2 = 3$ demarcates systems that are well fit (to the left of the line) from those that are poorly fit (to the right of the line) based on the number of degrees of freedom in the fits.

to L_X , we assumed that each star in the EB contributes half of the observed F_X and then used the nominal distance to the EB in the relation $L_X = F_X \times 4\pi d^2$. The sources we used for F_X are the ROSAT All-Sky Survey (Voges et al., 1999), the XMM-Newton Serendipitous Source Catalog (Watson et al., 2009), or measurements we made ourselves based on publicly available observations from the Chandra X-ray Observatory, and are indicated in each case in the references in Table A.5. For five of the components (RS Cha A and B, TY CrA A and B, and Par 1802 B), the measured $H\alpha$ and/or X-ray emission is very weak and as such these objects are below the range of applicability defined by Stassun et al. (2012) for the empirical relations; we do not attempt to correct these objects' properties.

With the δT_{eff} and δR in hand for each star, we re-fit each system using the same parameters and goodness-of-fit metrics as before. The results are shown in Figure 8 for the EB systems that have the requisite $H\alpha$ or X-ray measurements. In each case the χ^2 is shown as a function of the age of the isochrone considered for the fit to the six measured quantities. For this illustration we have used only the Dartmouth 2014 models. Solid lines corresponding to fits with no corrections for

activity are compared separately with the goodness of fit after corrections based on either $H\alpha$ or X-rays. It is not at all clear that the activity corrections systematically improve the fits, as one might have expected from the somewhat limited experience with similarly active main-sequence EBs (e.g., Feiden & Chaboyer, 2012b, 2013). The corrections do improve the fits to the brown dwarf system 2MASS J05352184–0546085 (hereafter 2M 0535–05), to ASAS 052821+0338.5, and especially to JW 380, but make less of a difference for RX J0529.4+0041, which is already well fit without the adjustments. The match to CoRoT 223992193 is actually made worse (although the quality of the fit is still acceptable after the activity corrections), while that of Par 1802 is not improved and the results for V1174 Ori are mixed, depending on whether the corrections are based on $H\alpha$ or X-rays. Perhaps the only pattern we see is the obvious one, which is that activity corrections yield older ages because the activity-corrected radii are smaller, making these young stars appear farther along in their contraction phase.

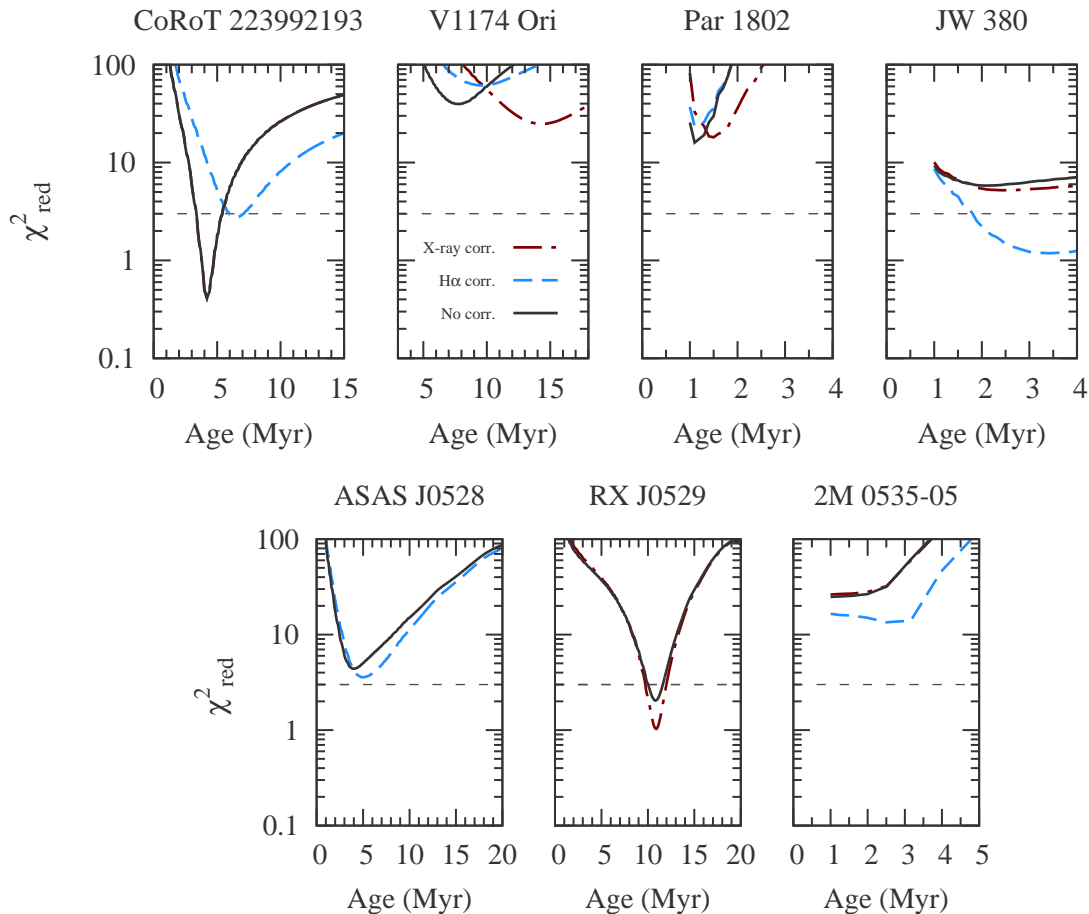


Figure 8: Change in the quality of the best-fit isochrones (black solid line) when the measured stellar radii and T_{eff} are adjusted for the observed $H\alpha$ (maroon dash-dotted line) and/or X-ray activity (light-blue dashed line) (Table A.5) using the empirical relations of Stassun et al. (2012).

4.4. Lithium

For seven of our EB systems there are measurements available of the strength (equivalent width) of the lithium absorption line at $\lambda 6708 \text{ \AA}$, for one or both components. When reported in the original sources the corresponding Li abundances have been taken as published; otherwise we have computed them from the published equivalent widths using the curve-of-growth tables of Pavlenko & Magazzù (1996), after properly accounting for the light contribution of each component. All values are listed in Table A.5.

Note that we have not included the secondary components of Par 1802 and JW 380 in the compilation, even though they have published Li equivalent widths, because these stars are cooler than the range of T_{eff} included in the Pavlenko & Magazzù (1996) tables. The curve-of-growth tabulation provided by Palla et al. (2007) does extend down to these very cool temperatures, but does not quite reach the $\log g$ values required,

and is computed only under LTE. Additionally, this more recent abundance scale seems very different, and would yield values of $\log N(\text{Li})$ an order of magnitude larger for some of our stars. For consistency with previous work we have chosen to use the standard scale of Pavlenko & Magazzù (1996), and we therefore exclude the secondaries of Par 1802 and JW 380 from consideration.

The measurements are compared with models of Li depletion in Figure 9. We find theoretical predictions from standard models to be broadly consistent with the observed abundances for the higher-mass stars in our sample that are expected to be undepleted (left panel, stars in the range $1.12\text{--}1.38 M_{\odot}$).

For the two components of V1174 Ori (middle panel) there is good agreement with non-magnetic models, whereas magnetic models seem to be excluded. Reasonably good agreement is seen as well between the measured and predicted Li abundance

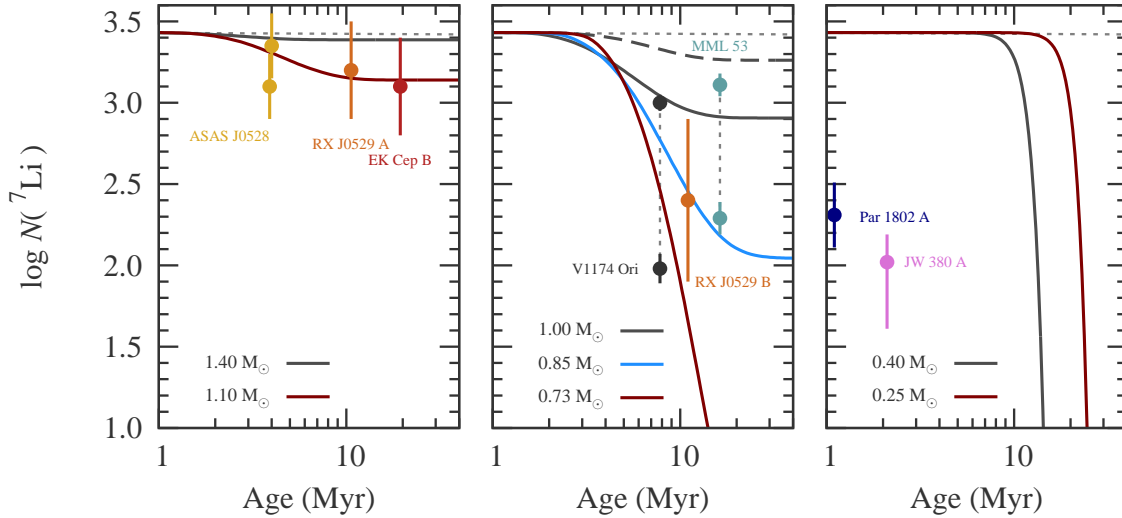


Figure 9: Models of lithium depletion from the Dartmouth 2014 model set compared to the measured Li abundances for stars with $M > 1 M_{\odot}$ (left), $0.5 < M < 1.0 M_{\odot}$ (middle), and $M < 0.5 M_{\odot}$ (right). The data are plotted at the best-fit age from the Dartmouth 2014 isochrone fits (Table 3). Model curves are shown for masses corresponding to specific stars in each panel for direct comparison. The primary and secondary components of V1174 Ori and MML 53 (middle panel) are connected with dotted lines. All models are non-magnetic, except the grey dashed track in the middle panel, which is a $1 M_{\odot}$ model with a 1 kG surface magnetic field.

for RX J0529.4+0041 B and MML 53 A from standard models. For V1174 Ori, one would predict an age of 9.5 Myr based on Li depletion curves compared to the 7.8 Myr age predicted from fitting the fundamental properties. Shifting the age to 9.5 Myr produces comparatively worse agreement with the fundamental properties. At 9.5 Myr, models over-predict the primary mass by $0.07 M_{\odot}$ (5σ) and the primary radius by $0.11 R_{\odot}$ (10σ). Marginal improvements are found with the other properties in our fit. Looking instead at how the models perform at the exact quoted masses at 9.5 Myr, one finds the models under-predict the primary and secondary radius by about 10% and 3% (13σ , 3σ), respectively, while the primary T_{eff} is under-predicted by 2% ($< 1\sigma$) and the temperature difference is under-predicted by nearly 50% (7σ).

In the right panel of Figure 9 the measured Li abundances for the primaries of Par 1802 and JW 380 are seen to be significantly lower than predicted by either standard or magnetic models for their mass and age, by more than an order of magnitude. These are also the youngest systems in the sample with measured Li abundances. In Sect. 5 we revisit these Li abundance patterns, and in particular the apparent over-depletion of Par 1802 and JW 380, including possible systematic errors in the absolute scale for the Li abundances (see above).

The problematically low Li abundances for the lowest-mass systems (Par 1802, JW 380) notwithstand-

ing, we emphasize that broadly there is very good agreement between the observed and predicted Li abundances in the EB sample (left and middle panels). In particular, it is striking that both components of V1174 Ori agree reasonably well with the expected Li abundance pattern for coeval stars at an age of ~ 10 Myr, despite the other properties of the system being very poorly fit by the same models (see Figure 6). The same is true of MML 53, although the primary’s Li is slightly elevated relative to the $1.0 M_{\odot}$ model prediction by $\sim 3\sigma$. The primaries of MML 53 and V1174 Ori have nearly identical masses of $\approx 1.0 M_{\odot}$, and comparable ages of ~ 10 Myr, so might be expected to have nearly identical Li abundances. Interestingly, the primary of MML 53 is more rapidly rotating than is the primary of V1174 Ori (by virtue of the shorter orbital period, and assuming tidal synchronization), thus it is possible that the slightly higher Li abundance of the MML 53 primary is the result of rotationally induced activity retarding its Li destruction, as suggested by Somers & Pinsonneault (2014) to explain the spread of Li abundances in young clusters.

4.5. Coevality of EBs in clusters

Two of the EBs in our sample (V615 Per and V618 Per) are members of the young h Persei cluster (distance ≈ 2200 pc), and three others (Par 1802, JW 380, and 2M 0535–05) are members of the ONC (distance ≈ 420 pc). These EBs therefore permit a test

of the degree to which the stars in these two regions are truly coeval. Figure 10 shows the result of comparing these EBs to single isochrones near the nominal cluster ages of 1–2 Myr (ONC) and ~ 13 Myr (Perseus). For the ONC systems, there is no single isochrone that satisfactorily fits all three systems at once. Collectively the stars are consistent with ages of 1–2 Myr, although the JW 380 system appears to be ~ 0.5 –1 Myr older than Par 1802. For the two Perseus systems, three of the four stars are consistent with a single cluster age of ~ 13 Myr; however, the lowest mass star (V618 Per B) does not lie on the same isochrone, although the discrepancy is at less than the 2σ level.

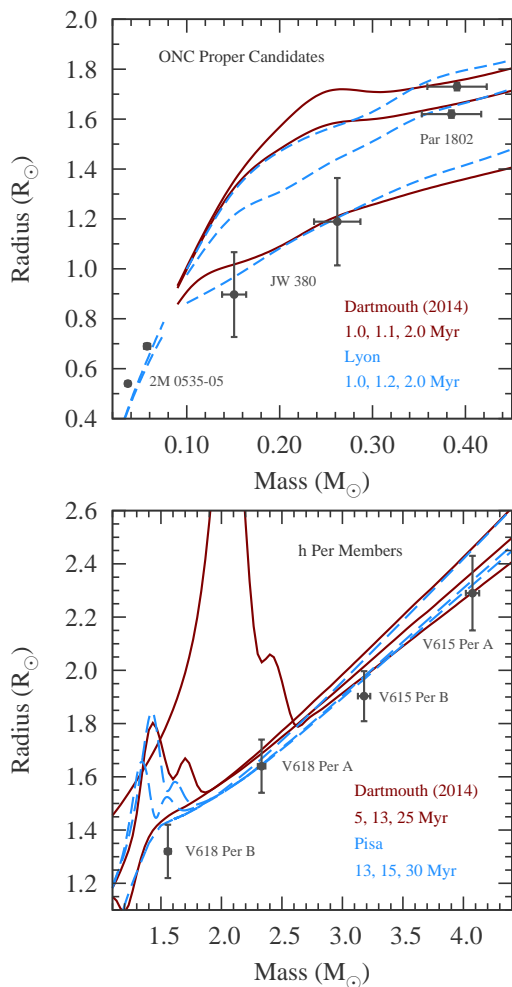


Figure 10: Mass-radius diagram for the EBs in our sample that are members of cluster populations expected to be coeval. *Left:* Orion Nebula Cluster systems compared against Dartmouth 2014 and Lyon ($\alpha_{\text{MLT}} = 1.9$) isochrones for a range of ages. The 2M 0535–05 system is compared against $\alpha_{\text{MLT}} = 1.0$ Lyon models, which are the only ones considered in this review that reach such low masses. *Right:* Similar diagram for the two h Per systems, with a comparison against Dartmouth 2014 and Pisa isochrones.

Thus, based on these comparisons, and to the extent that the measurements are accurate, it appears that the members of these two clusters are not strictly coeval, but exhibit an apparent age spread of ~ 1 Myr. For the ONC, this represents a spread of $\sim 50\%$ in age across the EB systems. Interestingly, however, the individual systems seem to be much more coeval, with the inferred ages of the individual stars agreeing to $\sim 20\%$. This is similar to the findings of Kraus & Hillenbrand (2009), who showed using binaries in Taurus that the stars within binaries are much more coeval ($\sim 40\%$) than are the binaries considered in aggregate ($\sim 150\%$).

5. Discussion

In the previous section, we examined the degree to which the measured properties of the benchmark EBs agree with the predictions of PMS stellar evolution models. We find very mixed results. The fits of the various stellar models to each system are visually summarized in Figure 7, where we show the goodness-of-fit metric for each system as a function of total system mass. Systems to the left of the vertical line are those with a total χ^2 that is equal to or better than that expected for a good fit. A number of the systems in the sample can clearly be considered to be very well matched to most of the theoretical models for two coeval stars. These systems (to the left of the vertical line) include: V618 Per, V615 Per, RS Cha, and CoRoT 223992193. At the same time, other systems are not well matched by most (or any) of the theoretical models. These systems (to the right of the vertical line) include: TY CrA, EK Cep, ASAS 052821+0338.5, RX J0529.4+0041, V1174 Ori, Par 1802, JW 380, and 2M 0535–05.

As is evident from Figure 7, the tendency for some systems to be better fit by the stellar models is not simply a function of the system mass. In this section, we consider how the goodness of fit (or lack thereof) for the different systems might be understood through the action of various possible physical effects, and we close with a summary of the implications of this discussion for the efficacy of current theoretical models in the context of observational studies of young stars and star-forming regions.

5.1. Activity: Effects of Magnetic Fields

Magnetic activity is an obvious culprit to consider for explaining the discrepancies between the observed and predicted properties for many of the PMS EBs. Most of the stars are observed to be active (in $H\alpha$ and/or X-rays;

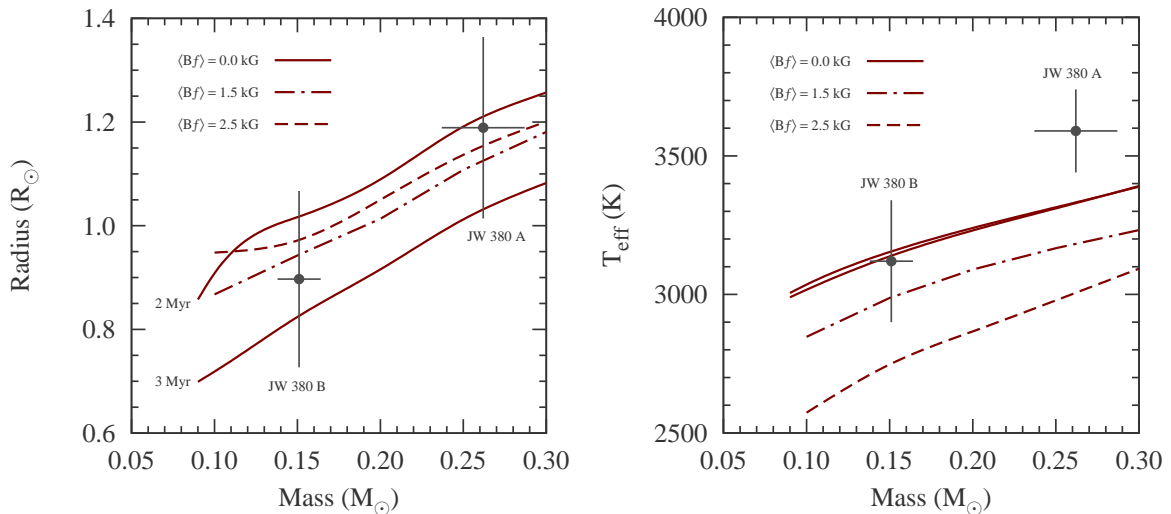


Figure 11: Effect of magnetic fields on the predicted radii (left) and temperatures (right) for the components of JW 380 according to the Dartmouth 2014 models, for three different field strengths as labeled, at an age of 3 Myr. A non-magnetic isochrone for 2 Myr is also shown.

see Table A.5) and none of the stellar models currently incorporate magnetic field effects in their “standard” versions. In Sect. 4.3 (see Fig. 8), we found that while a few of the systems (ASAS 052821+0338.5, JW 380, and 2M 0535–05) do appear to be largely “fixed” through the use of empirical activity adjustments to the stellar radii and T_{eff} (Stassun et al., 2012), the other active systems are either not significantly helped by these empirical corrections (V1174 Ori, Par 1802) or else are actually made somewhat worse (CoRoT 223992193).

Stassun et al. (2012) previously showed that application of their empirical activity corrections to 2M 0535–05, comprising two brown dwarfs at a nominal age of 1–2 Myr, substantially improved that system’s agreement with standard model predictions, so the improvement found here for that system is not surprising. However, although the observed reversal of T_{eff} with mass present in this binary (Stassun et al., 2006a, 2007; Gómez Maqueo Chew et al., 2009) could be mitigated, the models still predicted a primary mass that was too low given the observed luminosity. Conversely, models of the secondary star predicted too large of a mass after activity corrections. The reason that the models still predict incorrect masses is that the activity corrections altered both the primary’s T_{eff} and its radius, leaving the luminosity effectively constant, whereas the luminosity must increase to find agreement with the models. Issues with the primary could potentially be rectified by assuming that spots only influence the observed luminosity and T_{eff} , but do not impart changes in the radii. Spots that evolve on a short timescale com-

pared to the object’s thermal timescale might be consistent with this picture. However, Mohanty & Stassun (2012) performed detailed spectral modeling of the 2M 0535–05 system during eclipse to argue that spots are probably not strong in the system and spot models appear unable to explain the observed T_{eff} reversal. In any case, this would not provide better consistency with the secondary’s mass. The disagreement may therefore point to yet unresolved systematic problems with sub-stellar structure models at PMS ages that even activity corrections cannot fully rectify.

The effects of strong surface and/or internal magnetic fields have recently been incorporated into the Dartmouth models using a physically consistent treatment within the framework of mixing length theory (MLT) (Lydon & Sofia, 1995; Feiden & Chaboyer, 2012b). An example of what these models predict for the impact of magnetic fields in JW 380 is illustrated in Figure 11. Two 3 Myr magnetic model isochrones are shown, one where both stars have a surface magnetic field $\langle Bf \rangle = 1.5$ kG and the other with $\langle Bf \rangle = 2.5$ kG. Peak magnetic field strengths within the stars are 10–20 kG. The magnetic isochrones show the expected increase in stellar radii and reduction in T_{eff} as convective flux is reduced. Although the magnetic isochrones produce better consistency between the two stars at an age of 3 Myr in the M - R plane, suppressing the T_{eff} s produces worse agreement in the M - T_{eff} plane. We find that this result is typical when trying to fit magnetic models to the PMS EB population.

In summary, the effects of magnetic activity are ex-

pected to be ubiquitous among low-mass PMS stars such as those that comprise our benchmark sample. However, the expected magnitude of the effect on the radii and T_{eff} for most of the stars is not expected to be large enough to fully explain the significant discrepancies seen in many of the EBs. Activity effects alone do not appear to be the principal solution to the problem of the poorly fit EBs.

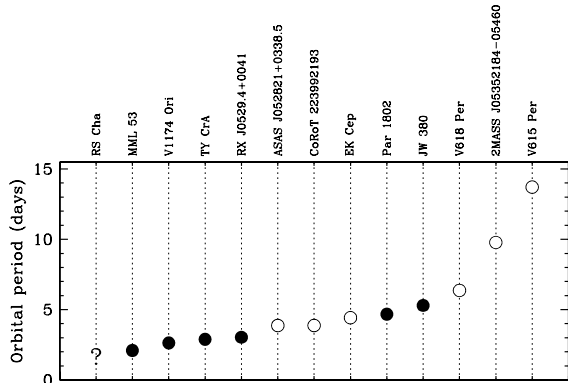


Figure 12: PMS EB sample sorted by orbital period. Filled circles represent systems with known tertiary components, and open circles those with no known third stars. Evidence for a tertiary in the case of RS Cha still needs to be confirmed.

5.2. Lithium: Probing effects on internal stellar structure

We have found that there is fairly good agreement between the observed and predicted Li abundances in the EB sample (see Section 4.4). This is interesting and perhaps counterintuitive considering the large discrepancies between the observed and predicted stellar properties for many of the EBs. It is not clear how the stellar global properties (i.e., T_{eff} and R) can be altered without also causing larger discrepancies in Li abundance than observed. Here we simply note this interesting observation and leave its explanation to future investigation.

An additional factor that can influence the Li depletion, as well as the global properties of PMS stars, is the efficiency of convection (see, e.g., Hillenbrand & White, 2004; Young et al., 2001), typically parametrized in stellar evolution models in terms of the mixing length parameter. While the models evaluated here (and indeed most of the published models) adopt a value of α_{MLT} appropriate for the Sun, Tognelli et al. (2012) have considered non-solar (lower) values of α_{MLT} . Their study included three of the EBs in the present sample as well as several somewhat older clusters, but the results for the EBs were largely inconclusive due to the small number of Li measurements and

the fact that the uncertainties are still relatively large in most cases.

Beyond the obvious choice of a solar-calibrated α_{MLT} for solar-mass stars at solar age, the specific choice of α_{MLT} in other contexts has long been a source of debate as there is a lack of empirical constraints to suggest what values are most appropriate in different evolutionary stages. Advancements in 3D radiation-hydrodynamic models and production of large grids of such models may help guide the development of models that do not adopt a single value for α_{MLT} , but employ a value that varies with stellar properties as it evolves (Freytag et al., 2012; Magic et al., 2013, 2014).

5.3. Tertiary Stars: Effects of Dynamical and Tidal Heating

A large number of the EBs in our benchmark sample are found to contain at least one additional stellar companion (Table 1). Indeed, six of the 13 systems have known tertiary stars, for a high fraction of triples to binaries of almost 90%³. Such a high occurrence of triples is not unexpected for this sample; most of the EBs have very short orbital periods, and in the field Tokovinin et al. (2006) finds that the occurrence of triples among binaries with orbital periods < 3 d is as high as 96%. Indeed, in the EB sample studied here, there is a tendency for the tertiary companions to be present among the EBs with the shortest orbital periods and absent among those with the longest periods (Figure 12).

Comparing the goodness of fit for the stellar mass EBs with known tertiaries to those without tertiaries (Figure 13), we find a striking difference, with the triple systems being systematically poorly fit whereas the non-tertiary systems are in general well fit by at least one of the models. The exceptions to this trend are EK Cep and, to a lesser degree, ASAS J052821+0338.5.⁴ EK Cep is not known to have a tertiary component but its properties are very poorly fit by all of the stellar models (see Figure 6). In addition, the brown-dwarf EB 2M 0535–05 is not well fit by the models (only the Lyon models go low enough in mass to attempt a fit) despite not having a known tertiary. While improved through the application of empirical activity corrections, it remains problematic, perhaps because of

³There is some evidence that RS Cha may also be a triple from small changes in the systemic velocity and in the $O - C$ residuals of the eclipse timings (Böhm et al., 2009; Woollands et al., 2013), but this has yet to be confirmed.

⁴We exclude MML 53 here as it is not sufficiently well characterized to permit a stringent constraint; see Sect. 4.2 and Appendix A.

deficiencies in the models at substellar masses (see Section 5.1). EK Cep and ASAS J052821+0338.5 remain problematic for other as-yet unidentified reasons. Perhaps they are triples after all but have not yet been identified as such.

Nonetheless, it appears that the tendency to triplicity among the PMS EB sample cannot be ignored as a likely important factor in their failure to be well fit by standard PMS stellar models. Broadly speaking, there are two possible explanations for this: observational systematics associated with the presence of third light in the EB analysis, and physical effects associated with the additional dynamics of a three-body system.

We believe that observational systematics are unlikely to be the dominant explanation. In each case in which contamination of the EB photometry by third light has been suspected, the effect has been accounted for in the analysis in one way or another, at least to first order (see Appendix A). Any residual effects would mostly influence the inclination angle, and have a much smaller impact on the relative radii and temperatures. The absolute masses would be largely unaffected by residual errors in the inclination angle. Additional blending of the spectral lines from the unrecognized presence of a third star would also have a minimal effect on the masses, which are determined mostly from observations at the orbital quadratures, where line blending is the smallest.

In contrast, there are reasons on physical grounds to expect that the dynamics of these three-body systems may help to explain why these systems are not well fit by the standard stellar models. For example, Reipurth & Mikkola (2012) have demonstrated that the rapid dynamical evolution of triple systems during the PMS phase can explain the occurrence and hierarchical nature of triples in the field. In those simulations, the triple systems initially begin non-hierarchically, but then through a highly dynamical set of chaotic interactions, rapidly “unfold” dynamically on a timescale of 1–10 Myr, leaving behind a very tight inner binary and a wide tertiary.

There are two dynamical effects in this picture that could directly impact the binary and the properties of the stars that comprise it. One effect is the input of energy from the tertiary’s orbit into one or both of the inner binary stars. The second effect is the tidal interaction of the two inner binary stars if they become tight enough at an early evolutionary stage when their radii are large compared to their orbital separation.

We perform here a simple order-of-magnitude estimate to evaluate potential effects of three-body dynamics on the properties of the stars in an inner binary, rep-

resenting the EB that we observe, with an outer tertiary star. The conceptual argument is that the energy contained in the orbit of the tertiary about the inner binary is of the same order of magnitude as the total amount of energy that would need to be injected into one or both of the stars of the inner binary to produce the observed luminosity difference compared to the standard model predictions. This requires that the deposited energy is rapidly dissipated within the stars from large-scales to small-scales so as to be able to quickly provide internal support against gravity (e.g., via convective turbulence; Zahn, 2005).

Consider V1174 Ori, perhaps one of the worst fit EBs in the sample. We can compute the observed stellar luminosities using the derived fundamental properties and the Stefan-Boltzmann law. This yields $L_A = 0.65L_\odot$ and $L_B = 0.17L_\odot$ for the primary and secondary, respectively. There is then a luminosity difference $\Delta L = 0.47L_\odot$ between the two components. Stellar models, on the other hand, predict a luminosity difference of only $\Delta L_{\text{model}} \approx 0.24L_\odot$ during the PMS contraction of two stars with masses similar to V1174 Ori. One can conclude that the primary is either too luminous or the secondary too faint for the system’s age, or some combination of the two.

For the purposes of this calculation, we assume that the primary is too luminous by $\sim 0.2 L_\odot$ and that the secondary is more-or-less “normal.” We also make the simplistic assumption that the tertiary star injects energy into the primary star only, at a rate equal to the primary’s observed over-luminosity. If the tertiary has an orbital period of $P_{\text{orb}} \sim 10^4$ yr, as is not uncommon for tertiary stars in hierarchical triples, then at an earlier time in the dynamical evolution of the system its orbit will have been shorter by, say, a factor of 100. In any case, over the course of subsequent tertiary orbits of 10^2 – 10^4 yr, the primary will not have time to relax back to its original configuration on the Hyashi track between subsequent periastron passages of the tertiary. This is because the Kelvin-Helmholtz timescale, t_{KH} , is $\sim 10^7$ yr. The star will contract somewhat after each periastron passage, but for simplicity we assume it does not. To maintain the primary at $L_A = 0.65L_\odot$, the tertiary must inject $Q_{\text{tidal}} \sim 0.2L_\odot \times 10^{2-4}\text{yr} \sim 10^{42-44}$ erg of heat in each orbital pass. Here, L_\odot is the solar luminosity and the last factor is the tertiary orbital period.

By comparison, we can estimate the amount of energy contained in the tertiary’s orbit about the inner binary as the sum of the kinetic and potential energies of the inner binary and the tertiary: $E_{\text{orb}} = -GM_{\text{binary}}M_{\text{tertiary}}/2a$, where a is the orbital semi-major axis. Using Kepler’s third law we can rewrite this in

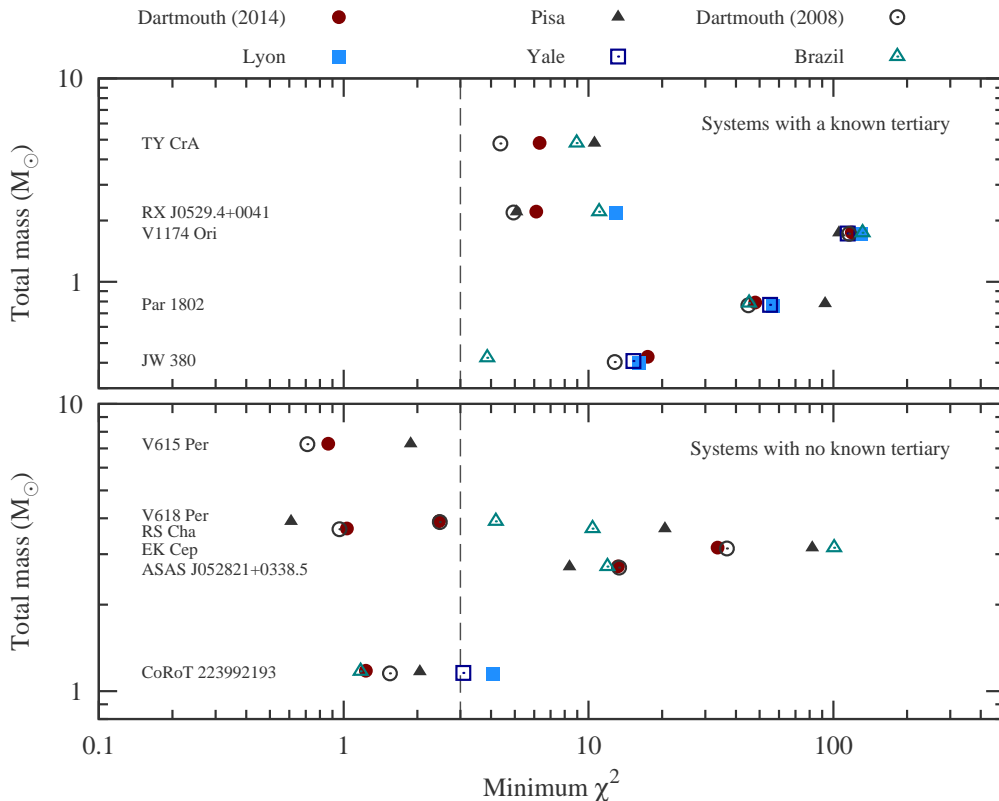


Figure 13: Best-fit χ^2 values for stellar mass EBs in our sample sorted according to the total mass of the system. The goodness of fit is shown with different symbols for each model used in each case (key on top). The vertical dashed line represents the expected χ^2 value based on the number of degrees of freedom, if the errors were Gaussian. (Top) Systems with a known tertiary component. (Bottom) Systems with no known tertiary component. The brown dwarf EB 2M0535–05, being substellar, is excluded from this diagram; see the text.

terms of the orbital period,

$$E_{\text{orb}} = -\frac{1}{2}\mu \left[\frac{2\pi G}{P} (M_{\text{binary}} + M_{\text{tertiary}}) \right]^{2/3}, \quad (2)$$

where $\mu = M_{\text{binary}}M_{\text{tertiary}} / (M_{\text{binary}} + M_{\text{tertiary}})$ is the reduced mass of the system, M_{binary} is the mass of the inner binary, and M_{tertiary} is the mass of the tertiary. Given an orbital period of 10^2 – 10^4 yr and $M_{\text{binary}} = 1.73M_{\odot}$, we estimate that $E_{\text{orb}} \sim 10^{42}$ – 10^{44} erg, depending on the tertiary mass. Table 4 gives the range of energies that are required to be deposited to generate the various luminosity differences we observe in V1174 Ori, and in two other systems. We list values of the orbital energy assuming a tertiary mass M_{tertiary} of 0.05, 0.10, or $0.50M_{\odot}$ orbiting the inner binary with a period of 10^2 , 10^3 , or 10^4 yr.

In general, the orbital energies available in the tertiary orbit are of the same order of magnitude as the total amount of energy that typically needs to be injected into one of the stars of the inner binary. This is a highly idealized scenario and the actual tidal interactions are far

more complex, but it is tantalizing that the energies are so similar. If the tertiary had an extremely strong and violent dynamical interaction with a star in the inner binary, it is possible that the rate of energy transfer vastly exceeded the total luminosity of the star in the inner binary. This could then deposit the requisite quantity of energy in the star in only a few encounters. However, it could also be that weaker, more regular encounters occurring over several Myr have a more lasting impact and allow the star to maintain a higher luminosity for longer due to continual injections of energy.

Finally, once the tertiary has sufficiently tightened the inner binary orbit, producing the short-period EB that we observe, tidal interaction between the two EB stars can potentially continue to inject heat into one or both of the EB stars. For example, Gómez Maqueo Chew et al. (2012) showed in the case of Par 1802 that tidal interaction between the two EB stars over the past ~ 1 Myr can account for the over-luminosity of $\sim 10^{26}$ W by the primary over the nearly equal-mass secondary. Par 1802 is one of the EB systems in our sam-

Table 4: Orbital energy (erg) for a tertiary companion of mass M_{tertiary} and orbiting with a period of 10^2 – 10^4 yr.

EB	M_{binary} (M_{\odot})	$M_{\text{tertiary}} = 0.05M_{\odot}$			$0.10M_{\odot}$			$0.50M_{\odot}$		
		10^2 yr	10^3 yr	10^4 yr	10^2 yr	10^3 yr	10^4 yr	10^2 yr	10^3 yr	10^4 yr
V1174 Ori	1.73	2.9e+43	6.2e+42	1.3e+42	5.7e+43	1.2e+43	2.7e+42	2.7e+44	5.8e+43	1.2e+43
Par 1802	0.77	1.7e+43	3.6e+42	7.7e+41	3.3e+43	7.0e+42	1.5e+42	1.4e+44	3.1e+43	6.7e+42
JW 380	0.41	1.1e+43	2.3e+42	5.0e+41	2.1e+43	4.5e+42	9.7e+41	8.6e+43	1.8e+43	4.0e+42

ple possessing a known tertiary component. While Gómez Maqueo Chew et al. (2012) did not attempt to model the dynamical evolution of the system as a triple, they concluded that the direct tidal interaction of the EB stars was likely driven into its current configuration by the action of the tertiary in the recent past. Therefore it appears plausible, both qualitatively and in terms of the quantitative energetics discussed above, that the tertiaries in many of the PMS EBs have influenced the evolution of the stars either directly, through injection of tertiary orbital energy, or indirectly through tightening of the inner EB to the point that binary tidal interaction injects sufficient heat to alter the observed stellar properties.

5.4. Accretion: Effects of Accretion History

Some theoretical studies have argued that the detailed accretion histories of low-mass stars can be important in setting the physical properties of the stars during the PMS contraction phase (e.g., Siess & Forestini, 1996; Hartmann et al., 1997; Tout et al., 1999; Baraffe & Chabrier, 2010; Hosokawa et al., 2011; Baraffe et al., 2012). If true, calculations suggest that the effect could be quite dramatic, with a very “bursty” accretion history producing a change in the stellar radius by a factor of ~ 3 or more at ~ 1 Myr (e.g., Baraffe & Chabrier, 2010). In addition, the higher internal temperatures would lead to dramatically enhanced Li depletion, and thus could explain the apparently anomalously low Li abundances reported for some members of young star-forming regions (e.g., Palla et al., 2007). Thus, we may consider a scenario in which the EBs in our sample possessing tertiary components have undergone more bursty accretion episodes in the past, leading to discrepant stellar properties (undersized radii, increased T_{eff} , and under-luminosity) compared to standard models.

The apparently highly Li depleted JW 380 might be taken as circumstantial evidence of accretion effects. If we assume the system is younger than estimated by standard stellar models (1 Myr instead of 2 Myr, for instance), then one finds that both stars exhibit smaller

radii than predicted by models. Furthermore, the primary is hotter (by about 200 K) and less luminous than one would then expect from a 1 Myr isochrone. However, coupling this interpretation with the apparently high Li depletion depends critically on the adopted PMS curve-of-growth and Li abundance scale, which has large model uncertainties at the very cool T_{eff} of this low-mass system. The same concern regarding the Li abundance scale at cool T_{eff} applies to Par 1802, although in any case this system does not appear to exhibit properties consistent with episodic accretion predictions. In particular, despite the primary and secondary stars having a mass ratio very near unity, the primary is much hotter, larger, and more luminous than the secondary. To cause the secondary to be so much smaller than the primary, it would need to have undergone stronger accretion bursts than the primary, in which case the secondary should be significantly hotter than the primary, which is the opposite of what is observed. None of the other tertiary-hosting EBs in our sample exhibit strong Li depletion. Overall, there are no clear “smoking gun” signals in our EB sample of the predicted effects of accretion history.

5.5. Overall performance of PMS stellar models, and the H-R Diagram Revisited

In Section 4.1 we considered how well the various PMS stellar models are able to reproduce the known masses of the EB stars in the H-R diagram, as this is a basic use of the stellar models for observational studies of young stars and star-forming regions. We found that in general the model-inferred masses are accurate to $\sim 10\%$ for masses above $1 M_{\odot}$, but considerably less reliable (mass errors of 50–100%) below $1 M_{\odot}$ and with a tendency for the models to over-predict the masses for these low-mass stars. While these trends were found to be true for most or all of the models, there we did find some differences. For example, the Pisa and Brazil model sets exhibited the lowest scatter in the mass discrepancies below $1 M_{\odot}$, and especially the Brazil models showed the smallest mean offset in the inferred stellar masses (Table 2).

The relatively good performance of the Pisa models in particular might not be surprising considering that these models were specifically developed for application to the PMS. The relatively good performance of the Brazil models is interesting, as to our knowledge these have not been widely utilized in the literature. These models are the only representative of the ATON code among the model sets we have examined in this paper, and they appear to perform on par with the other more widely used model sets. Perhaps this is due to the limited set of outputs provided in this model series for direct comparison to observables (notably colors and magnitudes).

However, and most importantly, there is a fundamental limitation to firmly assessing the efficacy of the models with the EB sample that we have considered in this paper. It is clear that EBs, and in particular those with tertiary companions (at least half of the sample), may not represent a directly comparable test of standard models of single stars.

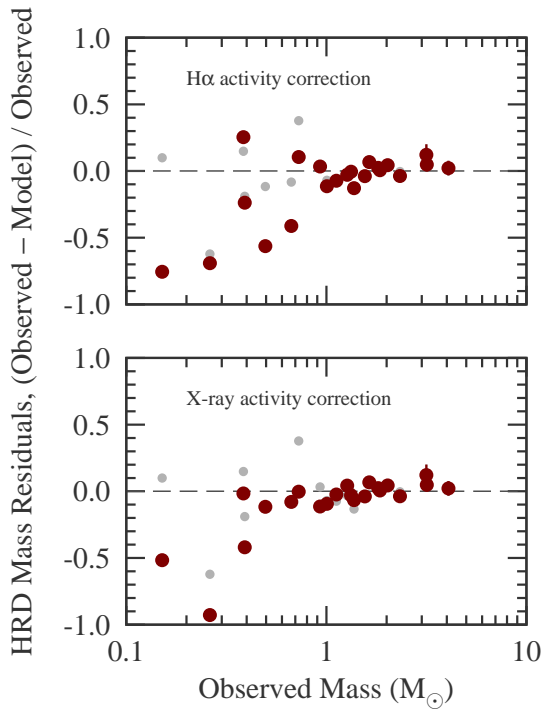


Figure 14: Normalized mass residuals between the measured EB masses and those inferred by the Dartmouth 2014 models in the H-R diagram, as a function of measured mass, after correction for activity effects on R and T_{eff} following Stassun et al. (2012). Results are shown separately for activity corrections based on H α (top) and X-rays (bottom). Residuals without corrections are represented with grey symbols.

Therefore, we revisit the performance of the stellar

models in predicting the measured EB stellar masses in the H-R diagram, but now accounting for activity effects and the presence of tertiaries. We again fit each of the model isochrones to the individual EB stars as in Section 4.1, but now adjust the observed stellar T_{eff} and R for activity effects as in Section 4.3. The result is shown in Figure 14 where we find that while there is some improvement in the model inferred masses for some objects, in general activity effects alone cannot fully reconcile the discrepancies in the inferred masses. This is especially noticeable at low masses, where empirically correcting the data for magnetic activity further degrades agreement between models and observations.

Next, we separate the EB sample into those systems bearing tertiaries versus those without, in Figure 15. Here we do not adjust the observed stellar properties for activity effects. We observe a striking result, namely that the stars not in triple systems have their masses very well reproduced by the models, to better than $\sim 10\%$ over the full range of stellar masses sampled (from $4.0 M_{\odot}$ down to $0.5 M_{\odot}$), whereas those in triple systems constitute all of the highly discrepant cases, with mass errors of 50% or more as noted earlier.

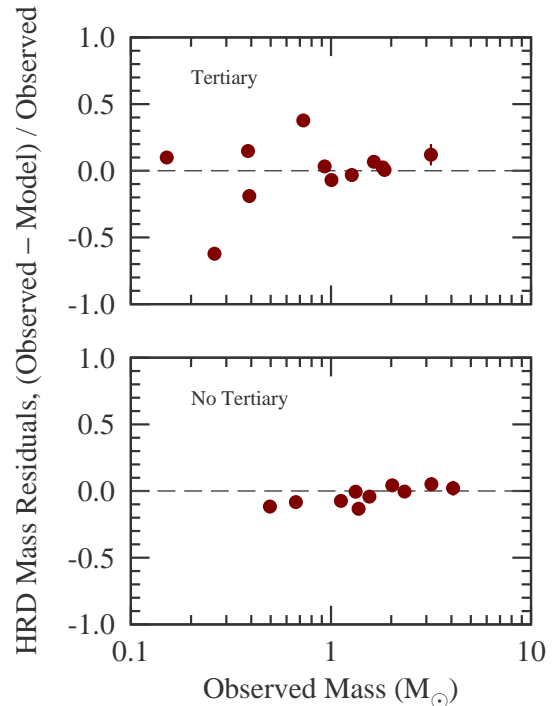


Figure 15: Normalized mass residuals from the Dartmouth 2014 models as in Figure 14, shown here without corrections for activity effects, and displayed separately for systems with and without known tertiary components.

There is a hint in the no-tertiary sample of a tendency

toward slightly over-predicted stellar masses at the low-mass end. Unfortunately, the lowest-mass stars are all in triple systems, and therefore we cannot determine with this sample whether the trend of over-predicted masses continues to the lowest masses, or whether the large mass discrepancies are entirely the result of effects associated with the tertiaries in those systems.

6. Conclusions and Future Work

We have performed a detailed assessment of the ability of various standard (solar-calibrated) PMS stellar evolution model sets to accurately reproduce the observed properties of a benchmark sample of 13 PMS EBs with masses in the range $0.04\text{--}4.0 M_{\odot}$ and with nominal ages ranging from ~ 1 to 20 Myr. The fundamental properties of the EBs, and the salient physical ingredients of the models, have been carefully compiled for future reference and use by the community. Through this exercise we have learned much about the interesting and complex physics of the PMS stage—particularly in PMS stars that are influenced by their companions—complexities that are definitively not yet incorporated in any standard PMS models.

Crucially, we have found that the presence of tertiary companions in many—perhaps most—of the PMS EBs appears in some way to corrupt the agreement of the observed stellar properties with the standard model predictions for young single stars. We have considered several mechanisms by which the tertiaries might do this, with direct injection of heat into one or both of the EB stars appearing to be the most plausible explanation. Indeed, we find that the energies of the tertiary orbits are comparable to that needed to potentially explain the scatter in the EB properties, perhaps through tidal interaction.

We find that the three EBs in the ONC are individually coeval to better than $\sim 20\%$, whereas in the aggregate they show an age spread of $\sim 50\%$. In other words, the two stars in each EB system are more coeval than are the EBs relative to one another. This may be the result of scatter in the EB properties due to the tertiaries. Alternatively, this could be taken as evidence for a real age spread across the ONC cluster. The apparently high Li depletion of JW 380 could be taken as additional evidence of an age for this system that is higher than average for the cluster. However, work is needed to firm up the Li abundance scale at such low T_{eff} for PMS stars to verify that the Li abundance in this system (and in Par 1802) is in fact highly depleted.

More generally, we find broadly very good agreement between the observed and predicted Li abundances in the EB sample, including for EBs that are otherwise

very poorly fit by the stellar models in terms of the other physical properties. This suggests that whatever the mechanism is by which the EB stars’ surface properties are affected, the internal structure of the stars is not sufficiently altered to cause comparably large problems with the Li abundances. At the same time, detailed comparisons between EB stars of comparable mass and age (i.e., V1174 Ori A and MML 53 A, both with mass $\sim 1.0 M_{\odot}$ and age ~ 10 Myr) show slightly different Li abundances, with the more rapidly rotating MML 53 being less depleted, suggesting that rotationally suppressed Li depletion may be inducing spreads in Li abundances as early as ~ 10 Myr (Somers & Pinsonneault, 2014).

The aforementioned results refer only to models with a solar-calibrated α_{MLT} , since those are the most commonly available. Use of a different value for α_{MLT} will have an impact on the ability of standard models to fit the EB data (e.g., Tognelli et al., 2012; Hillenbrand & White, 2004; Young et al., 2001). In this review we have adopted the solar-calibrated α_{MLT} primarily for the sake of uniformity so that we might better tease out the other dominant effects that bear upon the performance of the models against measured stellar properties. Advancements in 3D radiation-hydrodynamic models are needed to guide the development of stellar evolution models that employ a value for α_{MLT} that varies in a physically appropriate way as the stars evolve.

As surveys of young stars and star-forming regions continue, there will be opportunities to enhance the sample of the benchmark PMS EBs. Some of the existing PMS EBs need to have complete analyses performed, in particular MML 53 (which still does not have definitive individual radii determined) and the recently discovered EBs in the ONC by Morales-Calderón et al. (2012). There is also in general a need for more careful and consistent measurement of activity tracers in these EBs. In this paper, we have attempted to recover the activity information from the primary literature on the EB sample used here, but this was difficult in some cases. Still, we remain convinced that activity effects alone are unlikely to fully reconcile the discrepancies. The reason is that for a subset of the EBs we do already have reliable activity measurements, and the model versus data differences are not uniformly improved using the empirical activity corrections that have been developed based on main-sequence samples (e.g. Stassun et al., 2012). It appears that PMS stars are instead dominated by other effects tied in some way to the presence of tertiary companions, as we have discussed (e.g., tidal interaction).

Similarly, while our main analysis made use of the T_{eff} differences measured directly from the light curve

solutions, our assessment of the models versus the data in the H-R diagram necessarily still depends on the absolute T_{eff} of the primary stars, which could be subject to systematic uncertainties due to different T_{eff} scales adopted by various authors. Finally, in general the original EB discovery papers have not performed detailed analyses of the metallicities of the EBs, so we have resorted to assuming solar metallicity for most of the systems in our analysis. This is probably a reasonable assumption, especially for the EBs that are members of young clusters whose overall metallicities do have some observational basis for being very nearly solar. But in general metallicity is expected to be a factor in the predicted stellar properties, so this should ideally be carefully investigated on a system-by-system basis in the future. Along the same lines, efforts should be made whenever possible to measure the Li abundance for both components of young EBs, or at least to report their equivalent widths along with the light ratios between the stars, to enable the abundances to be computed.

While the focus of PMS EB discovery papers is usually to establish the absolute masses, radii, and temperatures of the stars, observers are strongly encouraged to report also other intermediate quantities such as mass ratios, temperature ratios (or differences), and radius ratios, which can usually be determined to higher accuracy and precision than the absolute properties and consequently provide more stringent constraints on models, as we have shown here. Reliable measurements for PMS EB stars are still so few in number that it is particularly important also to fully document any efforts to control systematic errors, or at least to assess their importance, in order to enable a critical judgment of the reliability of the analysis.

Just as observers should strive to publish all of the available information that can be pulled from the data, so too should modelers. Aside from the most basic quantities (R , T_{eff} , L), modelers should strive to publish a wide array of secondary quantities, such as lithium abundance and properties of the stellar convection zone, including convective turnover times—both local and globally averaged. Such quantities as the radius of gyration and internal structure constants may also be of interest to those testing stellar models. Additionally, modelers are encouraged to develop extensive, high resolution model grids, in both mass and metallicity, that minimize the need for interpolation into sub-grid regimes. This includes making available both detailed mass tracks and isochrones. Observers would also benefit from development of grids that cover “non-standard” parameter spaces (e.g., Tognelli et al., 2011;

Spada et al., 2013), such as varying α_{MLT} , deuterium abundances, solar composition, magnetic fields, and accretion physics. Of course, computation of such extensive grids is daunting given the number of tunable parameters, but effort toward this ideal should be made nonetheless.

Finally, it is clear that the triplicity of these systems, and the resulting dynamics, cannot be ignored in future efforts to understand and fully utilize these most fundamental stellar benchmarks. Indeed, when we consider only EB stars that are not members of triple systems, we find that current PMS stellar models are able to faithfully recover the measured stellar masses to better than $\sim 10\%$ in the H-R diagram, down to $0.5 M_{\odot}$. It is possible that there is a systematic tendency for the models to over-predict the stellar masses in the H-R diagram at low masses, but unfortunately the current benchmark EB sample is dominated by triple systems at the lowest masses, precluding our ability to properly assess this possibility. We do not believe that observational issues are to blame for the poor fits of the stellar models to the EBs in triple systems, but rather it is very likely that there are real astrophysical effects driving this fundamental finding. Failing to account for the presence of triples in the EB sample leads to inferred masses in the H-R diagram that are incorrect by 50–100%.

We hope that these insights will motivate additional theoretical work into the effects and observable consequences of magnetic fields and activity, of accretion history, and especially into the dynamical evolution of binary and triple systems including the effects of N-body and tidal interaction. To the extent that most or all young stars likely experience accretion early in their evolution and/or dynamical interactions especially in cluster environments, these issues will likely continue to be salient in our understanding of PMS stellar evolution and in our ability to test and calibrate the theoretical stellar models that are so central to our paradigm of star formation.

Acknowledgments

KGS acknowledges NSF grants AST-1009810 and AST-0849736. GT acknowledges partial support from NSF grant AST-1007992. GAF acknowledges NSF grant AST-0908345 and the William H. Neukom 1964 Institute for Computational Science at Dartmouth College, which both supported the development of the magnetic Dartmouth stellar evolution code. This research has made use of NASA’s Astrophysics Data System, the SIMBAD database and the VizieR catalog access tool, both operated at CDS, Strasbourg, France, and

the ROSAT data archive tools hosted by the High Energy Astrophysics Science Archive Research Center (HEASARC) at NASA's Goddard Space Flight Center. The research has also made use of data obtained from the Chandra Data Archive and the Chandra Source Catalog, and software provided by the Chandra X-ray Center (CXC) in the application packages CIAO, ChIPS, and Sherpa. We thank Scott Wolk for his assistance in the use of those tools.

References

References

Alecian E., Catala C., van't Veer-Menneret C., Goupil M.-J., Balona L., 2005, *A&A*, 442, 993
 Alexander D. R., Ferguson J. W., 1994, *ApJ*, 437, 879
 Allard F., Hauschildt P. H., 1995, *ApJ*, 445, 433
 Allard F., Homeier D., Freytag B., 2011, in *Astronomical Society of the Pacific Conference Series*, Vol. 448, 16th Cambridge Workshop on Cool Stars, Stellar Systems, and the Sun, Johns-Krull C., Browning M. K., West A. A., eds., p. 91
 Anders E., Grevesse N., 1989, *Geochim. Cosmochim. Acta*, 53, 197
 Andersen J., 1975, *A&A*, 44, 445
 —, 1991, *A&ARv*, 3, 91
 Asplund M., Grevesse N., Sauval A. J., 2005, in *Astronomical Society of the Pacific Conference Series*, Vol. 336, *Cosmic Abundances as Records of Stellar Evolution and Nucleosynthesis*, Barnes III T. G., Bash F. N., eds., p. 25
 Asplund M., Grevesse N., Sauval A. J., Scott P., 2009, *ARA&A*, 1
 Baraffe I., Chabrier G., 2010, *A&A*, 521, A44
 Baraffe I., Chabrier G., 2010, *A&A*, 521, A44
 Baraffe I., Chabrier G., Allard F., Hauschildt P. H., 1998, *A&A*, 412, 403
 —, 2002, *A&A*, 382, 563
 Baraffe I., Chabrier G., Gallardo J., 2009, *ApJ*, 702, L27
 Baraffe I., Vorobyov E., Chabrier G., 2012, *ApJ*, 756, 118
 Bate M. R., 2009, *MNRAS*, 392, 590
 Bell C. P. M., Naylor T., Mayne N. J., Jeffries R. D., Littlefair S. P., 2012, *MNRAS*, 424, 3178
 Bell R. A., Eriksson K., Gustafsson B., Nordlund A., 1976, *A&AS*, 23, 37
 Böhm T., Zima W., Catala C., Alecian E., Pollard K., Wright D., 2009, *A&A*, 497, 183
 Bressan A., Marigo P., Girardi L., Salasnich B., Dal Cero C., Rubele S., Nanni A., 2012, *MNRAS*, 427, 127
 Brott I., Hauschildt P. H., 2005, in *ESA Special Publication*, Vol. 576, *The Three-Dimensional Universe with Gaia*, Turon C., O'Flaherty K. S., Perryman M. A. C., eds., p. 565
 Caffau E., Ludwig H.-G., Steffen M., Freytag B., Bonifacio P., 2011, *SoPh*, 268, 255
 Canuto V. M., Mazzitelli I., 1991, *ApJ*, 370, 295
 Capilla G., Fabregat J., 2002, *A&A*, 394, 479
 Cargile P. A., Stassun K. G., Mathieu R. D., 2008, *ApJ*, 674, 329
 Casey B. W., Mathieu R. D., Suntzeff N. B., Walter F. M., 1995, *AJ*, 109, 2156
 Casey B. W., Mathieu R. D., Vaz L. P. R., Andersen J., Suntzeff N. B., 1998, *AJ*, 115, 1617
 Castellani F., Kurucz R. L., 2003, in *IAU Symposium*, Vol. 210, *Modelling of Stellar Atmospheres*, Piskunov N., Weiss W. W., Gray D. F., eds., p. 20P
 Chaboyer B., Kim Y.-C., 1995, *ApJ*, 454, 767

Chabrier G., Baraffe I., 1997, *A&A*, 327, 1039
 Chauvin G., Lagrange A.-M., Beust H., Fusco T., Mouillet D., Lacombe F., Pujet P., Rousset G., Gendron E., Conan J.-M., Bauduin D., Rouan D., Brandner W., Lenzen R., Hubin N., Hartung M., 2003, *A&A*, 406, L51
 Clausen J. V., Nordström B., 1980, *A&A*, 83, 339
 Covino E., Frasca A., Alcalá J. M., Paladino R., Sterzik M. F., 2004, *A&A*, 427, 637
 Covino E., Melo C., Alcalá J. M., Torres G., Fernández M., Frasca A., Paladino R., 2001, *A&A*, 375, 130
 Da Rio N., Robberto M., Soderblom D. R., Panagia N., Hillenbrand L. A., Palla F., Stassun K., 2009, *ApJS*, 183, 261
 Da Rio N., Robberto M., Soderblom D. R., Panagia N., Hillenbrand L. A., Palla F., Stassun K. G., 2010, *ApJ*, 722, 1092
 D'Antona F., Mazzitelli I., 1994, *ApJS*, 90, 467
 —, 1997, *MmSAI*, 68, 807
 D'Antona F., Ventura P., Mazzitelli I., 2000, *ApJ*, 543, L77
 di Criscienzo M., Ventura P., D'Antona F., 2009, *A&A*, 496, 223
 Dotter A., Chaboyer B., Jevremović D., Kostov V., Baron E., Ferguson J. W., 2008, *ApJS*, 178, 89
 Eggleton P. P., 1971, *MNRAS*, 151, 351
 —, 1972, *MNRAS*, 156, 361
 Eggleton P. P., Faulkner J., Flannery B. P., 1973, *A&A*, 23, 325
 Feiden G. A., Chaboyer B., 2012a, *ApJ*, 757, 42
 —, 2012b, *ApJ*, 761, 30
 —, 2013, *ApJ*, 779, 183
 Ferguson J. W., Alexander D. R., Allard F., Barman T., Bodnarik J. G., Hauschildt P. H., Heffner-Wong A., Tamanai A., 2005, *ApJ*, 623, 585
 Freytag B., Steffen M., Ludwig H.-G., Wedemeyer-Böhm S., Schaffenberger W., Steiner O., 2012, *Journal of Computational Physics*, 231, 919
 Gennaro M., Prada Moroni P. G., Tognelli E., 2012, *MNRAS*, 420, 986
 Gillen E., Aigrain S., McQuillan A., Bouvier J., Hodgkin S., Alencar S. H. P., Terquem C., Southworth J., Gibson N. P., Cody A., Lendl M., Morales-Calderón M., Favata F., Stauffer J., Micela G., 2014, *A&A*, 562, A50
 Girardi L., Bressan A., Bertelli G., Chiosi C., 2000, *A&AS*, 141, 371
 Gómez Maqueo Chew Y., Stassun K. G., Prša A., Mathieu R. D., 2009, *ApJ*, 699, 1196
 Gómez Maqueo Chew Y., Stassun K. G., Prša A., Stempels E., Hebb L., Barnes R., Heller R., Mathieu R. D., 2012, *ApJ*, 745, 58
 Gómez Maqueo Chew Y., Stassun K. G., Prša A., Mathieu R. D., 2009, *ApJ*, 699, 1196
 Gómez Maqueo Chew Y., Stassun K. G., Prša A., Stempels E., Hebb L., Barnes R., Heller R., Mathieu R. D., 2012, *ApJ*, 745, 58
 Grevesse N., Noels A., 1993, in *Origin and Evolution of the Elements*, Prantzos N., Vangioni-Flam E., Casse M., eds., pp. 15–25
 Grevesse N., Sauval A. J., 1998, *SSRv*, 85, 161
 Guenther D. B., Demarque P., Kim Y., Pinsonneault M. H., 1992, *ApJ*, 387, 372
 Hartmann L., Cassen P., Kenyon S. J., 1997, *ApJ*, 475, 770
 Hauschildt P. H., Allard F., Baron E., 1999a, *ApJ*, 512, 377
 Hauschildt P. H., Allard F., Ferguson J., Baron E., Alexander D. R., 1999b, *ApJ*, 525, 871
 Hebb L., Cegla H. M., Stassun K. G., Stempels H. C., Cargile P. A., Palladino L. E., 2011, *A&A*, 531, A61
 Hebb L., Stempels H. C., Aigrain S., Collier-Cameron A., Hodgkin S. T., Irwin J. M., Maxted P. F. L., Pollacco D., Street R. A., Wilson D. M., Stassun K. G., 2010, *A&A*, 522, A37
 Heiter U., Kupka F., van't Veer-Menneret C., Barban C., Weiss W. W., Goupil M.-J., Schmidt W., Katz D., Garrido R., 2002, *A&A*, 392, 619
 Henyey L. G., Vardya M. S., Bodenheimer P., 1965, *ApJ*, 142, 841

- Herbst W., Herbst D. K., Grossman E. J., Weinstein D., 1994, *AJ*, 108, 1906
- Hill G., Ebbighausen E. G., 1984, *AJ*, 89, 1256
- Hillenbrand L. A., 1997, *AJ*, 113, 1733
- Hillenbrand L. A., White R. J., 2004, *ApJ*, 604, 741
- Hosokawa T., Offner S. S. R., Krumholz M. R., 2011, *ApJ*, 738, 140
- Iglesias C. A., Rogers F. J., 1996, *ApJ*, 464, 943
- Irwin A. W., 2007, *The FreeEOS Code for Calculating the Equation of State for Stellar Interiors V: Improvements in the Convergence Method*
- Irwin J., Aigrain S., Hodgkin S., Stassun K. G., Hebb L., Irwin M., Moraux E., Bouvier J., Alapini A., Alexander R., Bramich D. M., Holtzman J., Martín E. L., McCaughrean M. J., Pont F., Verrier P. E., Zapatero Osorio M. R., 2007, *MNRAS*, 380, 541
- Irwin J., Aigrain S., Hodgkin S., Stassun K. G., Hebb L., Irwin M., Moraux E., Bouvier J., Alapini A., Alexander R., Bramich D. M., Holtzman J., Martín E. L., McCaughrean M. J., Pont F., Verrier P. E., Zapatero Osorio M. R., 2007, *MNRAS*, 380, 541
- Jeffries R. D., Jackson R. J., Briggs K. R., Evans P. A., Pye J. P., 2011, *MNRAS*, 411, 2099
- King J. R., Soderblom D. R., Fischer D., Jones B. F., 2000, *ApJ*, 533, 944
- Kraus A. L., Hillenbrand L. A., 2009, *ApJ*, 704, 531
- Krishna Swamy K. S., 1966, *ApJ*, 145, 174
- Kurucz R. L., 1991, in *NATO ASIC Proc. 341: Stellar Atmospheres - Beyond Classical Models*, Crivellari L., Hubeny I., Hummer D. G., eds., p. 441
- Landin N. R., Mendes L. T. S., Vaz L. P. R., 2009, *A&A*, 494, 209
- Landin N. R., Mendes L. T. S., Vaz L. P. R., 2010, *A&A*, 510, A46
- Landin N. R., Ventura P., D'Antona F., Mendes L. T. S., Vaz L. P. R., 2006, *A&A*, 456, 269
- López-Morales M., 2007, *ApJ*, 660, 732
- López-Morales M., Ribas I., 2005, *ApJ*, 631, 1120
- Lydon T. J., Sofia S., 1995, *ApJ*, 101, 357
- MacDonald J., Mullan D. J., 2010, *ApJ*, 723, 1599
- , 2012, *MNRAS*, 421, 3084
- Magic Z., Collet R., Asplund M., Trampedach R., Hayek W., Chiavassa A., Stein R. F., Nordlund Å., 2013, *A&A*, 557, A26
- Magic Z., Weiss A., Asplund M., 2014, *ArXiv e-prints*
- Marigo P., Aringer B., 2009, *A&A*, 508, 1539
- Martín E. L., Rebolo R., 1993, *A&A*, 274, 274
- Mathieu R. D., Baraffe I., Simon M., Stassun K. G., White R., 2007, in *Protostars & Planets V*, pp. 411–425
- Mayne N. J., Naylor T., 2008, *MNRAS*, 386, 261
- Mihalas D., 1978, *Stellar atmospheres*, 2nd edn. W. H. Freeman and Co., San Francisco, CA
- Mihalas D., Dappen W., Hummer D. G., 1988, *ApJ*, 331, 815
- Mohanty S., Stassun K. G., 2012, *ApJ*, 758, 12
- Montalbán J., D'Antona F., Kupka F., Heiter U., 2004, *A&A*, 416, 1081
- Morales J. C., Ribas I., Jordi C., 2008, *A&A*, 478, 507
- Morales J. C., Ribas I., Jordi C., Torres G., Gallardo J., Guinan E. F., Charbonneau D., Wolf M., Latham D. W., Anglada-Escudé G., Bradstreet D. H., Everett M. E., O'Donovan F. T., Mandushev G., Mathieu R. D., 2009, *ApJ*, 691, 1400
- Morales-Calderón M., Stauffer J. R., Stassun K. G., Vrba F. J., Prato L., Hillenbrand L. A., Terebey S., Covey K. R., Rebull L. M., Terndrup D. M., Gutermuth R., Song I., Plavchan P., Carpenter J. M., Marchis F., García E. V., Margheim S., Luhman K. L., Angione J., Irwin J. M., 2012, *ApJ*, 753, 149
- Mullan D. J., MacDonald J., 2001, *ApJ*, 559, 353
- Palla F., Randich S., Pavlenko Y. V., Flaccomio E., Pallavicini R., 2007, *ApJL*, 659, L41
- Palla F., Stahler S. W., 1993, *ApJ*, 418, 414
- , 1999, *ApJ*, 525, 772
- Pavlenko Y. V., Magazzù A., 1996, *A&A*, 311, 961
- Pietrinferni A., Cassisi S., Salaris M., Castelli F., 2004, *ApJ*, 612, 168
- Plez B., 1992, *A&AS*, 94, 527
- Pols O. R., Tout C. A., Eggleton P. P., Han Z., 1995, *MNRAS*, 274, 964
- Popper D. M., 1980, *ARA&A*, 18, 115
- , 1987, *ApJL*, 313, L81
- Reipurth B., Mikkola S., 2012, *Nature*, 492, 221
- Ribas I., 2003, *A&A*, 398, 239
- Ribas I., Jordi C., Torra J., Giménez Á., 2000, *MNRAS*, 313, 99
- Rogers F. J., Nayfonov A., 2002, *ApJ*, 576, 1064
- Saumon D., Chabrier G., Van Horn H., 1995, *ApJS*, 99, 713
- Siess L., Dufour E., Forestini M., 2000, *A&A*, 358, 593
- Siess L., Forestini M., 1996, *A&A*, 308, 472
- Simon M., Dutrey A., Guilloteau S., 2000, *ApJ*, 545, 1034
- Simon M., Obbie R. C., 2009, *AJ*, 137, 3442
- Soderblom D. R., Hillenbrand L. A., Jeffries R. D., Mamajek E. E., Naylor T., 2013, *ArXiv e-prints*
- Somers G., Pinsonneault M., 2014, *ArXiv e-prints*
- Southworth J., Maxted P. F. L., Smalley B., 2004, *MNRAS*, 349, 547
- Spada F., Demarque P., Kim Y.-C., Sills A., 2013, *ApJ*, 776, 87
- Stassun K. G., Ardila D. R., Barsony M., Basri G., Mathieu R. D., 2004, *AJ*, 127, 3537
- Stassun K. G., Kratter K. M., Scholz A., Dupuy T. J., 2012, *ApJ*, 756, 47
- Stassun K. G., Mathieu R. D., Cargile P. A., Aarnio A. N., Stempels E., Geller A., 2008, *Nature*, 453, 1079
- Stassun K. G., Mathieu R. D., Mazeh T., Vrba F. J., 1999, *AJ*, 117, 2941
- Stassun K. G., Mathieu R. D., Valenti J. A., 2006a, *Nature*, 440, 311
- , 2007, *ApJ*, 664, 1154
- Stassun K. G., van den Berg M., Feigelson E., Flaccomio E., 2006b, *ApJ*, 649, 914
- Stempels H. C., Hebb L., Stassun K. G., Holtzman J., Dunstone N., Glowienka L., Frandsen S., 2008, *A&A*, 481, 747
- Swenson F. J., Faulkner J., Rogers F. J., Iglesias C. A., 1994, *ApJ*, 425, 286
- Tognelli E., Degl'Innocenti S., Prada Moroni P. G., 2012, *A&A*, 548, A41
- Tognelli E., Moroni P. G. P., Degl'Innocenti S., 2011, *A&A*, 533, A109
- Tokovinin A., Thomas S., Sterzik M., Udry S., 2006, *A&A*, 450, 681
- Tomkin J., 1983, *ApJ*, 271, 717
- Torres G., 2013, *Astronomische Nachrichten*, 334, 4
- Torres G., Andersen J., Giménez A., 2010, *A&ARv*, 18, 67
- Torres G., Ribas I., 2002, *ApJ*, 567, 1140
- Tout C. A., Livio M., Bonnell I. A., 1999, *MNRAS*, 310, 360
- VandenBerg D. A., Swenson F. J., Rogers F. J., Iglesias C. A., Alexander D. R., 2000, *ApJ*, 532, 430
- Vaz L. P. R., Andersen J., Casey B. W., Clausen J. V., Mathieu R. D., Heyer I., 1998, *A&AS*, 130, 245
- Ventura P., D'Antona F., Mazzitelli I., 2008, *Ap&SS*, 316, 93
- Vitense E., 1953, *ZA*, 32, 135
- Voges W., Aschenbach B., Boller T., Bräuninger H., Briel U., Burkert W., Dennerl K., Englhauser J., Gruber R., Haberl F., Hartner G., Hasinger G., Kürster M., Pfeiffermann E., Pietsch W., Predehl P., Rosso C., Schmitt J. H. M. M., Trümper J., Zimmermann H. U., 1999, *A&A*, 349, 389
- Watson M. G., Schröder A. C., Fyfe D., Page C. G., Lamer G., Mateos S., Pye J., Sakano M., Rosen S., Ballet J., Barcons X., Barret D., Boller T., Brunner H., Brusa M., Caccianiga A., Carrera F. J., Ceballos M., Della Ceca R., Denby M., Denkinson G., Dupuy S., Farrell S., Frascchetti F., Freyberg M. J., Guillout P., Hambaryan V., Maccacaro T., Mathiesen B., McMahon R., Michel L., Motch C., Osborne J. P., Page M., Pakull M. W., Pietsch W., Saxton R.,

- Schwöpe A., Severgnini P., Simpson M., Sironi G., Stewart G., Stewart I. M., Stobart A.-M., Tedds J., Warwick R., Webb N., West R., Worrall D., Yuan W., 2009, *A&A*, 493, 339
- Windmilller G., Orosz J. A., Etzel P. B., 2010, *ApJ*, 712, 1003
- Woollands R. M., Pollard K. R., Ramm D. J., Wright D. J., Böhm T., 2013, *MNRAS*, 432, 327
- Young P. A., Mamajek E. E., Arnett D., Liebert J., 2001, *ApJ*, 556, 230
- Zahn J.-P., 2005, in *Astronomical Society of the Pacific Conference Series*, Vol. 333, *Tidal Evolution and Oscillations in Binary Stars*, Claret A., Giménez A., Zahn J.-P., eds., p. 4

Appendix A. Notes on Individual PMS EB Systems

We describe here the particulars of the 13 pre-main sequence eclipsing binaries discussed in the main paper, explaining the sources of the mass, radius, and effective temperature measurements presented in Table 1. Because our goal is to provide meaningful comparisons with stellar evolution models, our primary concern is the accuracy of the results for each system, rather than the stated precision in the original publications. Consequently, we have examined each binary critically, and in some cases we have re-derived the stellar properties and/or adjusted their uncertainties to better reflect both the quality and quantity of the observations, as well as any complicating factors in the analysis. One of the most obvious for this sample is the presence of distortions in the light curve due to spots, which can evolve with time and can seriously compromise the accuracy of the radii (see, e.g., Windmilller et al., 2010). In about half of the systems the photometry is also contaminated to various degrees by “third light”. A more subtle problem that is often overlooked is degeneracies between several of the fitted parameters, most notably between the relative radii. The radius *sum* is usually well determined, but the *ratio* is much harder to establish accurately. This is commonly seen in partially eclipsing systems with similar components, and the best way to overcome the problem is to make use of an external constraint such as a spectroscopic light ratio (see, e.g., Andersen, 1991), by either imposing it on the light curve solution, or at least checking for consistency between the photometric and spectroscopic values. This has not always been possible for the systems below. As a result of these difficulties, and despite our best efforts to take them into account, the uncertainties that are reported may still be somewhat optimistic in some cases as they do not fully account for all systematic errors. This should be kept in mind when evaluating the fits to stellar evolution models discussed in the text.

In three cases (EK Cep, RS Cha, V1174 Ori) a similarly critical examination of the original sources and revision of the stellar parameters was carried out by

Torres et al. (2010), and we have simply adopted their values here.

In addition to compiling the usual fundamental properties of the binary components (M , R , T_{eff}), we have made an effort to extract from the original bibliographic sources measurements that are differential in nature, because they are usually more accurate as well as more precise, and therefore provide better and stronger constraints on stellar evolution models. One of these is the temperature difference between the primary and secondary, ΔT_{eff} . This quantity can typically be determined much more accurately from the light curve solutions than spectroscopically because it is tied directly to difference in the depths of the eclipses, which is relatively easy to measure in most cases. Individual temperatures, on the other hand, are more prone to systematics stemming from uncertainties in the absolute temperature scale for PMS stars. While errors for ΔT_{eff} are only rarely reported, we have reconstructed them here from the published information or by adopting a conservative estimate of the uncertainty in the temperature ratio, usually 0.01 unless otherwise noted. The ratio of the masses ($q \equiv M_B/M_A$) is typically also better determined than either of the individual masses, and was taken directly from the original sources, when published, or else derived from the velocity semi-amplitudes and their uncertainties. We have not collected or made use of the radius ratios from the literature because of the potential for systematics noted above, because they are seldom reported, and because it is not possible to recover their true errors from those of the individual radii.

V615 Per and V618 Per. These two EBs are members of the young open cluster h Per, for which various studies in the literature indicate a metallicity near solar, although with some scatter. The light curves analyzed by Southworth et al. (2004) are uncomplicated, and the solutions were constrained using the spectroscopic light ratio, at least for V615 Per. We have adopted the absolute masses, mass ratios, and radii from that source, along with their uncertainties. Similarly for the primary temperature, which is based on spectral disentangling. The temperature difference (and resulting secondary T_{eff}) was derived by us on the basis of the measured ratio of the central surface brightness (J_s) from the light curve fits along with the limb-darkening coefficients and the calibration by Popper (1980), and is considered more accurate than can be determined from the spectra.

TY CrA. The primary is a Herbig Be star. The light curve analysis of this system is complicated not only

Table A.5: Activity and other properties of young EBs

Star	Age (Myr) Dist (pc)	Comp	$\log N(\text{Li})^a$	$\text{H}\alpha$ EW (\AA) ^b F_X ($\text{erg s}^{-1} \text{cm}^{-2}$) ^d	$\log L_{\text{H}\alpha}/L_{\text{bol}}$	$\log L_X/L_{\text{bol}}$	[Fe/H] ^c References ^e
V615 Per	13	A	(0.0)
	2200	B	1,2
TY CrA	3	A	-5.37 ^f	...
	100	B	...	1.6×10^{-12}	...	-3.94 ^f	3,4,5
V618 Per	13	A	(0.0)
	2200	B	1,2
EK Cep	20	A	-4.80 ^f	$+0.07 \pm 0.05^g$
	150	B	3.1 ± 0.3	6.6×10^{-14}	...	-3.82	2,6,7,8,9,10,11
RS Cha	6	A	-5.47 ^f	$+0.17 \pm 0.01$
	100	B	...	3.0×10^{-13}	...	-5.46 ^f	6,12,13,14,15
ASAS J052821+0338.5	10	A	3.10 ± 0.20	... / 1	...	-3.24	-0.15 ± 0.20^h
	280	B	3.35 ± 0.20	5.0×10^{-13}	-3.98	-3.06	16,17
RX J0529.4+0041	10	A	3.2 ± 0.3	-3.39	(0.0)
	325	B	2.4 ± 0.5	3.4×10^{-13}	...	-2.97	18,19
V1174 Ori	10	A	3.00 ± 0.05^i	0.4 / 4.2	-4.42	-3.12	(0.0)
	390	B	1.98 ± 0.09^i	2.1×10^{-13}	-3.80	-2.55	6,20
MML 53	15	A	3.11 ± 0.07^i	-3.49	...
	136	B	2.29 ± 0.10^i	9.5×10^{-13}	...	-3.01	17,21,22
CoRoT 223992193	3-6	A	...	5.6	-3.45	-3.19	(-0.15)
	800	B	...	2.5×10^{-14}	-3.60	-2.94	11,23,24
Par 1802	1-2	A	2.31 ± 0.13^i	1	-4.40	-3.31	(0.0)
	420	B	...	8.8×10^{-14}	-4.49 ^f	-3.10	25,26
JW 380	1-2	A	2.0 ± 0.3^i	13	-3.32	-3.71	(0.0)
	420	B	...	1.5×10^{-14}	-3.51	-3.22	27,28
2MASS J05352184-0546085	1-2	A	...	32.6 / 4.8	-3.47	-3.89	(0.0)
	420	B	...	1.0×10^{-15}	-4.30	-3.76	29

^a Abundance on the usual scale in which $\log N(\text{H}) = 12$.

^b Two values are listed when measured separately for the primary and secondary.

^c Values in parentheses are assumed for the parent cluster or association of the binary.

^d Values from the sources indicated in the last column, or measured here directly from publicly available Chandra observations. In the case of ASAS J052821+0338.5 the location of the ROSAT source is nominally $11.6''$ from the binary position, still within the $14''$ ROSAT error circle; for MML 53 the ROSAT source is $5.7''$ from the binary position, well within the ROSAT error circle.

^e Sources for the data presented here as well as in Table 1.

^f Value outside of the range in which the activity correction relations of Stassun et al. (2012) are valid.

^g Metallicity for the secondary. The primary star has $[\text{Fe}/\text{H}] = -0.24$ from a single line.

^h Average metallicity for the two components ($[\text{Fe}/\text{H}] = -0.2 \pm 0.2$ and $[\text{Fe}/\text{H}] = -0.1 \pm 0.2$, respectively).

ⁱ Computed here or in the original sources under NLTE using the tables of Pavlenko & Magazzù (1996).

References: 1. Southworth et al. (2004); 2. Popper (1980); 3. Casey et al. (1998); 4. Casey et al. (1995); 5. Vaz et al. (1998); 6. Torres et al. (2010); 7. Popper (1987); 8. Hill & Ebbighausen (1984); 9. Tomkin (1983); 10. Martín & Rebolo (1993); 11. Watson et al. (2009); 12. Andersen (1975); 13. Clausen & Nordström (1980); 14. Ribas et al. (2000); 15. Alecian et al. (2005); 16. Stempels et al. (2008); 17. Voges et al. (1999); 18. Covino et al. (2004); 19. Covino et al. (2001); 20. Stassun et al. (2004); 21. Hebb et al. (2011); 22. Hebb et al. (2010); 23. Gillen et al. (2014); 24. King et al. (2000); 25. Gómez Maqueo Chew et al. (2012); 26. Cargile et al. (2008); 27. Irwin et al. (2007); 28. Da Rio et al. (2009); 29. Gómez Maqueo Chew et al. (2009).

by the presence of significant light from a third, spatially unresolved spectroscopic component, but also by contamination from the reflection nebula NGC 6726/7 in which the object is embedded. The velocity of the third star and of the center-of-mass of the binary are variable, and there is also evidence of a light-travel time effect in the eclipse timing residuals. The secondary eclipse is very shallow (~ 0.03 mag). Additionally, the light curves (Vaz et al., 1998) show variability on several timescales from days to years. We have adopted the absolute masses, radii, and primary T_{eff} from the work of Casey et al. (1998), in whose analysis an attempt was made to constrain the radius ratio with external information from their spectra. We have taken the radius errors from the same source. However, our independent analysis of the original radial velocities from Casey et al. (1995) indicates significantly larger uncertainties for the masses, so we adopted those more conservative errors here. The primary T_{eff} of Casey et al. (1998) is based on color indices in the Strömgren system, and that of the secondary comes directly from the light-curve analysis. The error in the temperature difference was estimated as indicated above. Finally, adaptive optics imaging by Chauvin et al. (2003) has revealed a close companion at a separation of $0.29''$. If physically associated, it would be an M4 star, making the system at least quadruple.

EK Cep. The light curves of this system show no complications. The masses and radii have been taken directly from the compilation of Torres et al. (2010), which updates the work of Popper (1987), who in turn based his results on the light curves of Hill & Ebbighausen (1984) and the spectroscopy of Tomkin (1983). The secondary eclipse appears to be total, or nearly so, and the primary eclipse possibly annular, which tends to alleviate degeneracies between the individual component radii. The primary T_{eff} and its error have also been adopted from Torres et al. (2010). The secondary temperature was revised slightly here as done above for V615 Per and V618 Per. Martín & Rebolo (1993) derived an estimate of the chemical abundance of the cooler secondary star of $[m/H] = +0.07 \pm 0.05$, based on five metal lines. The system shows measurable apsidal motion.

RS Cha. This is classified as a Herbig Ae system and a member of the young η Cha cluster. We have adopted the masses and radii from the compilation of Torres et al. (2010); they are based on the spectroscopic work of Andersen (1975) and photometric analysis of Clausen & Nordström (1980). Non-radial (δ Sct-type) pulsations have been detected in the

primary and secondary of RS Cha, both photometrically (Clausen & Nordström, 1980) and spectroscopically (Alecian et al., 2005; Böhm et al., 2009). The effects on the light curves are small and were accounted for in the analysis of Clausen & Nordström (1980), which also makes use of the spectroscopic light ratio to lift the degeneracy in the radius ratio. We have adopted the primary T_{eff} from Ribas et al. (2000), which we have then combined with the temperature ratio reported by Clausen & Nordström (1980) to infer the secondary T_{eff} , as well as ΔT_{eff} along with its corresponding error. Claims of changes in the center-of-mass velocity of the binary (Woollands et al., 2013) and non-linear variations in the $O - C$ eclipse timing residuals (Böhm et al., 2009) that might be indicative of a third body in the system require confirmation (see Andersen 1975 and Alecian et al. 2005). The latter study provided an estimate of the metallicity as $[\text{Fe}/\text{H}] = +0.17 \pm 0.01$, with a rather small uncertainty.

ASAS J052821+0338.5. This system is likely a member of the Orion OB1a region onto which it is projected. The light curves show obvious distortions presumably due to spots. The analysis of Stempels et al. (2008) explored two different treatments of these distortions (rectification, and direct modeling), and found rather significant differences in the relative radii and T_{eff} from the two approaches. The authors noted that the radius ratio is rather poorly determined in this case, likely due to the partial nature of the eclipses and the lack of a spectroscopic constraint on the light ratio. Their final results, which we have adopted here, are based on the rectified light curves. However, in view of the sensitivity of the results to the methodology, our concerns about the accuracy of the radius ratio, and the fact that our independent reanalysis of the spectroscopy yields slightly different velocity semi-amplitudes (particularly for the primary), we have conservatively increased the uncertainties in the masses and especially those in the radii over those reported in the original analysis. The primary T_{eff} we have adopted comes from spectral disentangling performed by Stempels et al. (2008). The secondary T_{eff} and corresponding ΔT_{eff} derive from the light curve analysis. We have assigned an error to the latter quantity based on an assumed uncertainty in the T_{eff} ratio of 0.03, which is larger than in other cases to account for the issues described above. Rough metallicities were reported for the primary and secondary as $[m/H] = -0.2 \pm 0.2$ and $[m/H] = -0.1 \pm 0.2$. We have adopted the average here for the system.

RX J0529.4+0041. This EB in the Orion OB1a region has a visual companion at approximately $1.3''$, which is also seen spectroscopically (Covino et al., 2001) and is likely physically associated as it shares the same radial velocity. The light curves are significantly affected by spots, in addition to the contamination from third light. The analysis of Covino et al. (2004) attempted to correct for both effects through a combination of direct spot modeling and rectification. The eclipses are partial and the stars rather similar, which combined with the other difficulties just described makes it challenging to reach high accuracy in the relative radii. Although a spectroscopic light ratio is available that might help remove the degeneracy, it does not appear that this piece of external information was used in this case. The possibility of systematic errors in the radii therefore remains, as is also mentioned by the authors. We have adopted the masses for the two components and their uncertainties as published, as well as the nominal radii, but we have increased the radius errors to be conservative. Covino et al. (2004) inferred the primary T_{eff} from its spectral type and several calibrations, while the secondary T_{eff} comes directly from the light curve solution. We take those values here as published, with their corresponding uncertainties, along with an error for ΔT_{eff} of 50 K as reported. The metallicity is assumed here to be that of the parent population, i.e., near solar.

V1174 Ori. This Orion nebula cluster system is considered a likely member of the Orion OB1c subgroup. We have adopted the masses, radii, and temperatures from the compilation of Torres et al. (2010), who provided slight revisions of the values in the original work of Stassun et al. (2004). The primary temperature is based on an assumed spectral type of $K4.5 \pm 0.1$ and a standard calibration. The uncertainty in ΔT_{eff} listed in Table A.5 was derived by us from an assumed error of 0.01 in the temperature ratio. As in other cool systems the effects of spots are obvious, but were accounted for in the modeling of Stassun et al. (2004). Evidence for a third star in the system comes from extra light required to properly fit the *I*-band light curve, as well as a significant color excess that increases toward the red.

MML 53. This EB is a probable member of the Upper Centaurus-Lupus sub-association, in the region of the Sco-Cen OB complex. The light curves display significant distortions due to spots. Rectified versions were used in the preliminary analysis of Hebb et al. (2010), although full details were not reported. A third, spatially unresolved star was discovered spectroscopically by these authors, which is likely physically associated

with the EB and also affects the light curves at the level of about 15%. A subsequent analysis by Hebb et al. (2011) presented a spectroscopic orbit and minimum masses for the components, which include contributions to the errors from the potential effects of spots. A definitive study of this binary is still needed, preferably with more complete phase coverage in the spectroscopy. For the present paper we have derived the absolute masses from the $M \sin^3 i$ values of Hebb et al. (2011) and the inclination angle of 83.1° reported in their earlier study, to which we have assigned an uncertainty of 1° . Individual radii have not been reported, likely because of the difficulty in determining the radius ratio with the photometric material at hand. A spectroscopic constraint on the light ratio would also be helpful, but is lacking. The only quantity pertaining to the star sizes that we are able to derive for MML 53 based on the published information is the radius sum, $R_A + R_B$, which we calculated from the sum of the relative radii (with an assumed 3% error), the projected semimajor axis, and the inclination angle. The T_{eff} s reported by Hebb et al. (2010) rely on a joint fit of the light curve and a single spectrum, and were considered by those authors to be preliminary. We have assigned them an error of 100 K.

CoRoT 223992193. This system is deemed a member of the young open cluster NGC 2264, for which an estimate of the metallicity has been given as $[\text{Fe}/\text{H}] \approx -0.15$ (King et al., 2000). The high-quality and continuous 23.4-day light curve from *CoRoT* shows obvious rotational modulation from spots that are seen to change with time. These distortions were removed in the analysis of Gillen et al. (2014) prior to fitting for the photometric elements. To help eliminate correlations between the relative radii the authors constrained the fit using their measured spectroscopic light ratio. We have adopted their masses and radii here as published, together with their formal uncertainties. The effective temperatures of both stars were determined by those authors by comparing their spectra with synthetic templates via cross-correlation. We have assigned them conservative uncertainties of 200 K. The original study does not provide information on the temperature difference from the light-curve solution.

Par 1802. Another member of the Orion Nebula Cluster. The light curves show intrinsic variability due to spots, as well as contamination from the light of a third unresolved star (also possibly spotted), implying the system is triple. Both effects were accounted for in the light-curve solutions of Gómez Maqueo Chew et al. (2012). The parameters and uncertainties we list in Ta-

ble A.5 were adopted from that work, which uses the spectroscopic material from Cargile et al. (2008). The primary T_{eff} is based on an adopted luminosity ratio and a combined T_{eff} for the system based on the combined M2 spectral type. We have computed the uncertainty in ΔT_{eff} from that of the T_{eff} ratio given by Gómez Maqueo Chew et al. (2012) and a more conservative error of 0.01 in that quantity. The system has the peculiarity that even though the components are of similar mass their temperatures are rather different, leading to a large difference in luminosity in excess of 60%, perhaps due to tidal heating (see also Stassun et al., 2008).

JW 380. A likely member of the Orion nebula cluster. In their analysis of this EB Irwin et al. (2007) detected a spatially unresolved spectroscopic companion that is most likely physically associated, making this a triple system. Its contribution to the total light ($\sim 13\%$) was accounted for in the fit. The light curve was also rectified prior to fitting in order to rid it of significant distortions due to spots. The authors noted the strong degeneracy in the radius ratio, from the fact that the luminosity ratio was not constrained in the fit, and they cautioned about the possibility of systematic errors in their light-curve results beyond the formal uncertainties. Here we have adopted their absolute masses (and uncertainties) as published. We did the same for the radii, but in view of their warning we adopted the largest of the (strongly) asymmetric error bars. Although Irwin et al. (2007) did not attempt to infer the temperatures, they did quote a value for the primary based on its assumed spectral type (M1.5). We have adopted this value, and assigned it a conservative uncertainty of 200 K. The secondary temperature (along with ΔT_{eff} and its uncertainty) were inferred from the reported temperature ratio, to which we have attached a more conservative error of 0.02 than originally indicated.

2MASS J05352184–0546085. This is a rare pair of eclipsing brown dwarfs in the Orion nebula cluster. In the most recent analysis of Gómez Maqueo Chew et al. (2009) the effects of spots apparent in the light curves were accounted for in the modeling; they imply a rather large spot coverage on the primary ($\sim 65\%$). This system shows a surprising temperature reversal, in the sense that the more massive and larger primary star is cooler than the secondary (see also Stassun et al. 2006b and Stassun et al. 2007). We have adopted here the masses and radii as reported in the Gómez Maqueo Chew et al. (2009) study, along with their uncertainties. We have also taken the primary temperature (based on the assumed spectral type of $M6.5 \pm 0.5$) and its error from

these authors, and computed the secondary temperature and ΔT_{eff} using the reported temperature ratio with a more conservative error of 0.01.

Appendix B. Physical Ingredients of Stellar Models, and Notes on Discarded Models

The physical ingredients of the accepted and rejected model sets are summarized in Tables B.6 and B.7, respectively. Notes on the rejected model sets are provided below.

ATON. Models by D’Antona & Mazzitelli (1994, 1997) are still adopted for studies of low-mass PMS systems. Although these models lack non-grey surface boundary conditions, they are still the only PMS model set to implement a non-local treatment of convection. This treatment, known as Full Spectrum of Turbulence (FST; Canuto & Mazzitelli, 1991), makes these models relevant for discussions of low-mass stellar physics. There have been updates to the ATON code (version 3.x Ventura et al., 2008), which include, among other improvements, the addition of non-grey surface boundary conditions that use both standard mixing length theory and FST (Montalbán et al., 2004; di Criscienzo et al., 2009). Unfortunately, the only set of publicly available models for the updated ATON 3.x code are for metal-poor stars. Solar metallicity tracks, though they have been computed, have not been made publicly available.

Grenoble. Of the model sets excluded from our analysis, the Grenoble models by Siess et al. (2000) are arguably the most widely adopted. A primary reason for the exclusion of these models is their unique adoption of “semi-grey” surface boundary conditions. These semi-grey surface boundary conditions are an analytical fit to the thermal structure of non-grey atmospheres. The analytical fit to non-grey atmosphere data reproduces the original non-grey atmosphere structures to within about 20%, suggesting non-adiabatic conditions in the outer layers of cool stars are being captured, at least in part. Comparing the Siess et al. (2000) mass tracks to Dartmouth model mass tracks, which adopt non-grey surface boundary conditions (see Figure 1), we find that the Siess et al. (2000) tracks predict systematically hotter effective temperatures. This is the same effect one expects from the use of grey $T(\tau)$ atmosphere relations at low-masses (Chabrier & Baraffe, 1997), leading us to believe that the semi-grey approach may be more akin to grey surface boundary conditions than non-grey. The morphology of the Siess et al. (2000) $0.2 M_{\odot}$ track rather closely matches that of the Baraffe et al. (1998)

models, although significant differences can be seen at $0.5 M_{\odot}$, where the Siess et al. (2000) models deviate quite noticeably. Our evaluation was further complicated by the fact that the $1.0 M_{\odot}$ mass track does not reproduce the properties of the Sun, as evidenced in Figure 1(b), despite a solar calibration having been performed (Siess et al., 2000).

Padova. The latest version of the Padova stellar evolution code include all physics relevant for PMS work at higher masses (Girardi et al., 2000; Bressan et al., 2012). They adopt the latest solar abundance values (Caffau et al., 2011) and are available for a wide range of stellar masses and metallicities. However, their adoption of an Eddington $T(\tau)$ grey surface boundary condition gives them limited applicability for rigorous tests of the validity of physical inputs at lower masses.

BaSTI. The Bag of Stellar Tracks and Isochrones (BaSTI) code is another stellar evolution code that has been updated in the past decade (Pietrinferni et al., 2004). As was the case with the Padova code, BaSTI is applicable to a wide range of astrophysical problems, particularly population synthesis studies. It is excluded from the present study due to its use of grey surface boundary conditions (Krishna Swamy, 1966). This, as has been mentioned previously, gives the code limited applicability for detailed studies near the bottom of the H–R diagram.

Palla & Stahler. Models by Palla & Stahler (1993, 1999) were unique for their use of an empirically calibrated stellar birthline used to define initial conditions for young stars. This is in contrast to most stellar evolution codes that assume an arbitrarily large radius at a very young age (e.g., 1000 years) as an initial condition. As with many older codes, these models use grey boundary conditions and are not publicly available.

Swenson et al. Based on the Cambridge STARS code (Eggleton, 1971, 1972), the models by Swenson et al. (1994) were designed for studying lithium abundances in young stars. The original models were never updated beyond the original release and are increasingly difficult to acquire. Their legacy lives on, in part, through the Victoria stellar evolution models (e.g., VandenBerg et al., 2000). At the time of their creation, non-grey atmosphere codes that were suitable for low-mass and very-low-mass stars were just coming of age (Allard & Hauschildt, 1995), so these models were released with grey atmospheres only.

Table B.6: Properties of pre-main-sequence evolutionary track sets adopted for use in this review.

Track Set	Code Lineage	Masses (M_{\odot})	Metallicities (solar)	Surface Boundary Conditions (fit point; mixture)	Radiative Opacities (mixture)	EOS	Convection (solar α_{MLT})	D, Li Burning ^a ($X_D \times 10^5$)
Lyon	Lyon	0.02 – 1.5 (α_{MLT} dependent)	–0.5, 0.0 (GN93; 0.019)	non-gray, Allard & Hauschildt (1995) ($\tau_{\text{fit}} = 100$; GN93)	OPAL; AF94 (GN93)	SCvH95	MLT (1.9)	Separate, Yes (2.0)
Dartmouth 2008	YREC	0.08 – 5.0	–2.5 → 0.5 (GS98; 0.0169)	non-gray, Hauschildt et al. (1999a,b) non-gray, Castelli & Kurucz (2003) ($T(\tau_{\text{fit}}) = T_{\text{eff}}$; GS98)	OPAL; F05 (GS98)	FreeEOS CK95	MLT (1.938)	No, Separate (0.0)
Dartmouth 2014	YREC	0.08 – 5.0	–1.0 → 0.5 (GS98; 0.0169)	non-gray, Hauschildt et al. (1999a,b) non-gray, Castelli & Kurucz (2003) ($\tau_{\text{fit}} = 10$; GS98)	OPAL; F05 (GS98)	FreeEOS CK95	MLT (1.884)	Yes, Separate (2.0)
Brazil	ATON	0.085 – 3.8	0.0 (GS99; 0.0175)	non-gray, Allard & Hauschildt (1995) ($\tau_{\text{fit}} = 10$; GN93)	OPAL; AF94 (AG89; GN93)	OPAL96 MHD	MLT (2.0)	Yes, Separate (2.0)
Yale	YREC	0.1 – 1.25	–1.5 → 0.3 (GS98; 0.0163)	non-gray, Allard et al. (2011) ($\tau = \dots$; GN93)	OPAL; F05 (GS98)	SCvH95 OPAL05	MLT (1.875)	No, Separate (0.0)
Pisa	FRANEC	0.20 – 7.0	$Z = 0.0002 \rightarrow 0.03$ (AGS05; 0.01377)	non-gray, Brott & Hauschildt (2005) ($\tau_{\text{fit}} = 10$; GN93) non-gray, Castelli & Kurucz (2003) ($\tau_{\text{fit}} = 10$; GS98)	OPAL; F05 (AGS05)	OPAL06	MLT (1.68)	Yes*, Yes* (2.0, 4.0)

^a Deuterium (D) and lithium (Li) burning was assessed on two levels. First, do the models include light element burning (Yes or No)? Second, if they do include D and Li burning, is it performed within a larger nuclear reaction network (Yes), outside of the regular nuclear reaction network (Separate), or if it is unclear from reading the literature (Yes*).

References *Track set*: Lyon, Baraffe et al. (1998); Dartmouth 2008, Dotter et al. (2008); Dartmouth 2014, Feiden et al. (in prep); Brazil, Landin et al. (2010); Yale, Spada et al. (2013); Pisa, Tognelli et al. (2011); *Heavy element mixture*: AG89, Anders & Grevesse (1989); GN93, Grevesse & Noels (1993); GS98/99, Grevesse & Sauval (1998); AGS05, Asplund et al. (2005); AGSS09, Asplund et al. (2009); C11, Caffau et al. (2011); *Opacities*: AF94, Alexander & Ferguson (1994); F05, Ferguson et al. (2005); OPAL, Iglesias & Rogers (1996); *EOS*: EFF: Eggleton et al. (1973); MHD, Mihalas et al. (1988); PTEH, Pols et al. (1995); CK95, Chaboyer & Kim (1995); SCvH95, Saumon et al. (1995); OPAL, Iglesias & Rogers (1996); OPAL06, Rogers & Nayfonov (2002); FreeEOS, Irwin et al. (2007); *Convection*: MLT, Vitense (1953), Mihalas (1978), Henyey et al. (1965);

Table B.7: Properties of pre-main-sequence evolutionary track sets that were not adopted for this review.

Track Set	Code Lineage	Masses (M_{\odot})	Metallicities (solar)	Surface Boundary Conditions (fit point; mixture)	Radiative Opacities (mixture)	EOS	Convection (solar α_{MLT})	D, Li Burning ^a ($X_D \times 10^5$)
B12	Padova	0.10 – 12.0	0.0005 → 0.07 (C11; 0.015)	gray, Eddington $T(\tau)$ ($\tau_{\text{fit}} = 2/3$; C11)	OPAL; MA09 (C11)	FreeEOS	MLT (1.74)	Yes, Yes (?)
DM97	ATON	0.015 – 3.0	$Z = 0.01, 0.02$ (AG89; 0.019)	gray, Henyey et al. (1965) ($\tau_{\text{fit}} = 2/3$; AG89)	OPAL; AF94 (AG89; GN93)	MHD OPAL96	MLT, FST (1.5)	Separate, Separate (1.5, 2.5, 4.5)
DVD09 MDKH04	ATON	0.10 – 1.5	$-2.0 \rightarrow 0.0$ (GS99; 0.0175)	non-gray, Allard & Hauschildt (1995) ($\tau_{\text{fit}} = 3$; GN93) non-gray, Heiter et al. (2002) ($\tau_{\text{fit}} = 10$; GN93)	OPAL; F05 (GS99)	SCvH95 OPAL	MLT, FST (1.6)	Yes*, Yes* (2.0, 4.5)
PCSC04	BaSTI	0.50 – 10.0 (Z dependent)	$Z = 0.0001 \rightarrow 0.04$ (GN93; 0.0198)	gray, Krishna Swamy (1966) ($\tau_{\text{fit}} = 2/3$, GN93)	OPAL; AF94 (GN93)	FreeEOS	MLT (1.931)	No, Yes (0.0)
PS99	PS93	0.10 – 6.0	0.0 (0.02)	gray, Eddington $T(\tau)$ ($\tau_{\text{fit}} = 2/3$)	OPAL; AF94 (GN93)	EFF PTEH	MLT (1.5)	Separate, No (2.5)
SDF00	Grenoble	0.10 – 7.0	$Z = 0.01 \rightarrow 0.04$ (GN93; 0.02)	semi-gray ^b , Plez (1992) semi-gray ^b , Bell et al. (1976) semi-gray ^b , Kurucz (1991) ($\tau_{\text{fit}} = 10$, AG89)	OPAL; AF94 (GN93)	Augmented PTEH	MLT (1.605)	Yes*, Yes* (2.0)
SFRI94	STARS	0.15 – 5.0	$-0.5, 0.0$ (AG89; 0.0188)	gray, Eddington $T(\tau)$ ($\tau_{\text{fit}} = \dots$; AG89)	OPAL; A92 (AG89)	Augmented EFF	MLT (1.957)	No, Yes

^a Deuterium (D) and lithium (Li) burning was assessed on two levels. First, do the models include light element burning (Yes or No)? Second, if they do include D and Li burning, is it performed within a larger nuclear reaction network (Yes), outside of the regular nuclear reaction network (Separate), or if it is unclear from reading the literature (Yes*).

^b Siess et al. (2000) use neither a fully gray or fully non-gray approach. They calculate an analytical fit to the non-gray atmospheres to provide their surface boundary conditions. However, this fit does not completely reproduce the original non-gray atmosphere data (within 20%), thus we deem it a “semi-gray” approach.

References *Track set*: B12, Bressan et al. (2012); DM97, D’Antona & Mazzitelli (1994, 1997); DVD09, di Criscienzo et al. (2009); MDKH04, Montalbán et al. (2004); PCSC04, Pietrinfermi et al. (2004); PS93/99, Palla & Stahler (1993, 1999); SDF00, Siess et al. (2000); SFRI94, Swenson et al. (1994); *Heavy element mixture*: AG89, Anders & Grevesse (1989); GN93, Grevesse & Noels (1993); GS98/99, Grevesse & Sauval (1998); AGS05, Asplund et al. (2005); AGSS09, Asplund et al. (2009); C11, Caffau et al. (2011); *Opacities*: AF94, Alexander & Ferguson (1994); F05, Ferguson et al. (2005); OPAL, Iglesias & Rogers (1996); MA09, Marigo & Aringer (2009); *EOSs*: EFF, Eggleton et al. (1973); MHD, Mihalas et al. (1988); PTEH, Pols et al. (1995); OPAL, Iglesias & Rogers (1996); OPAL06, Rogers & Nayfonov (2002); FreeEOS, Irwin (2007); *Convection*: MLT, Vitense (1953), Mihalas (1978), Henyey et al. (1965); FST, Canuto & Mazzitelli (1991);